Supporting Information

Palladium Hydrazonato Complexes and their role in the Pd-Catalyzed Cross-Coupling Reactions of Hydrazones as Carbene Precursors

Francisco Villalba and Ana C. Albéniz*

IU CINQUIMA/Química Inorgánica. Universidad de Valladolid. 47071 Valladolid (Spain)]

Table of contents

1. Additional experimental details

1.1- Synthesis of [Pd(C_6F_5)(dppf)($NCCH_3$)](BF_4) (2c).

Equimolar amounts of [Pd(Br)(C_6F_5)(dppf)] (128.2 mg, 0.14 mmol) and $AgBF_4$ (27.5 mg, 0.14 mmol) were mixed in dry CH_3CN (10 mL) and stirred for 15 min at room temperature under nitrogen. The suspension was filtered through Kieselghur and the filtrate was evaporated to dryness. The resulting orange oil (**2c**) was characterized by NMR. The orange oil was triturated with diethylether and n-hexane until the formation of an orange solid that was filtered, washed with n-hexane and air-dried. Yield: 98 mg, (73 %). This solid is contaminated by small amounts of reorganization products.

^{1}H NMR (499.73 MHz, δ, $CDCl_3$): 7.79-7.67 (m, 10H, H^{arom}), 7.46-7.32 (m, 6H, H^{arom}), 7.17 (m, 4H, H^{arom}), 5.03 (s, 2H, H^{Cp}), 4.80 (s, 2H, H^{Cp}), 4.39 (s, 2H, H^{Cp}), 3.61 (s, 2H, H^{Cp}), 2.00 (s, 3H, NCMe). $^{13}C\{^1H\}$ NMR (125.67 MHz, δ, $CDCl_3$): 145.1 (m, $^1J_{C-F}$ = 225.6 Hz, CF_{ortho}), 138.5 (m, $^1J_{C-F}$ = 248.0 Hz, CF_{para}), 136.1 (m, $^1J_{C-F}$ = 249.1 Hz, CF_{meta}), 133.6 (d, J_{C-P} = 12.0 Hz, C^{arom}), 133.1 (d, J_{C-P} = 12.0 Hz, C^{arom}), 132.3 (C^{arom}), 132.1 (C^{arom}), 130.6 (d, $^1J_{C-P}$ = 63.0 Hz, C^{arom}), 129.7 (d, $^1J_{C-P}$ = 49 Hz, C^{arom}), 129.8 (d, J_{C-P} = 10.3 Hz, C^{arom}), 128.5 (d, J_{C-P} = 11.9 Hz, C^{arom}), 116.8 (N*C*Me), 78.2 (d, J_{C-P} = 12.8 Hz, C^{Cp}) 75.4 (d, J_{C-P} = 8.9 Hz, C^{Cp}), 74.9 (d, J_{C-P} = 9.6 Hz, C^{Cp}), 74.0 (d, J_{C-P} = 6.6 Hz, C^{Cp}), 73.5 (dd, $^1J_{C-P}$ = 64.7 Hz, J_{C-P} = 7.2 Hz, C^{Cp}), 68.0 (dd, $^1J_{C-P}$ = 55.8 Hz, J_{C-P} = 2.7 Hz, C^{Cp}), 1.9 (NC*Me*).* ^{19}F NMR (470.17 MHz, δ, $CDCl_3$): -119.65 (m, 2F, F_{ortho}), -153.5 (s, 4F, BF_4), -157.59 (t, J = 20.5 Hz, 1F, F_{para}), -160.21 (m, 2F, F_{meta}). $^{31}P\{^1H\}$ NMR (202.31, MHz, δ, $CDCl_3$): 36.86 (m, 1P), 18.28 (m, 1P). IR (neat, cm^{-1}): C_6F_5: 1499, 1040, 950, 742, 692; CH_3CN, 2292; BF_4^- 1045.

*The ^{13}C signal for the C_{ipso} of the C_6F_5 group could not be observed.

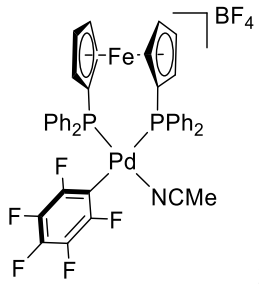

2c

1.2- Decomposition of the diazoalkane N_2CH-CH=CHPh and the N-tosylhydrazone 3.

1.2.1. Decomposition of N_2CH-CH=CHPh. A dichloromethane solution of the diazo compound (0.12 mmol) in dry CD_3CN (total volume 0.7 mL) was monitored by ^1H NMR at 298 K using 1,4-dioxane as an internal standard under a nitrogen atmosphere. The collection of data started 13 min after the preparation of the solution at 298 K. The decomposition products observed are 5-phenyl-1*H*-pyrazole,[1] and minor compounds such as the corresponding azine,[2] and trans-cinnamaldehyde. The identity of these compounds was determined by comparison of the ^1H NMR spectra of the decomposition monitorization to authentic samples prepared as reported in the literature.

The progress of the reaction is shown in Figure S1.

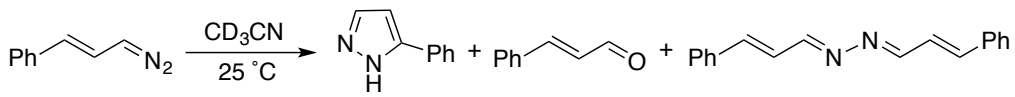

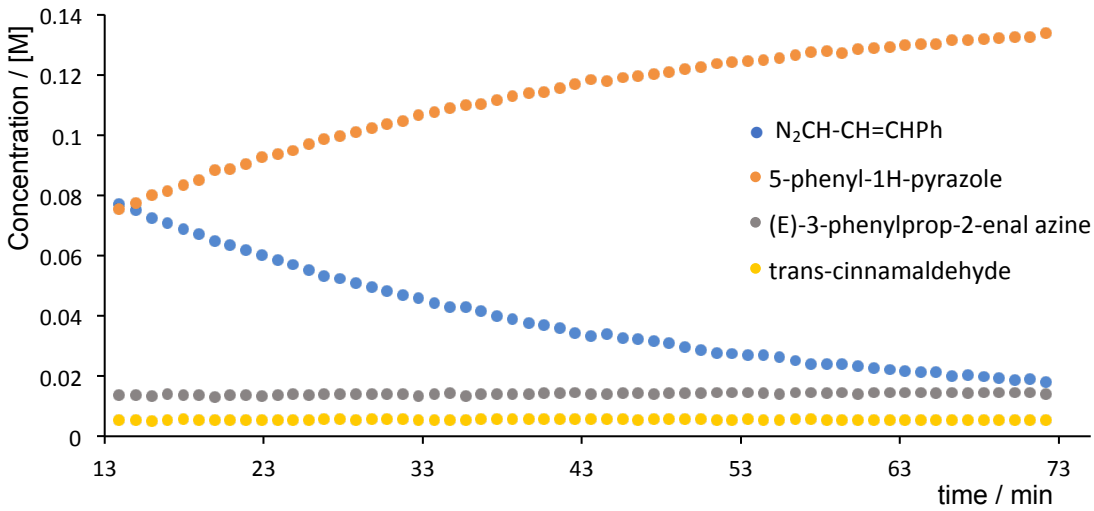

Figure S1. Plot of concentration vs time for the decomposition of the diazoalkane N_2CH-CH=CHPh in CD_3CN at 298 K.

1.2.2. Decomposition of the *N*-tosylhydrazonate. *N*-tosylhydrazone **3** (0.033 mmol), base (0.05 mmol), additive (0.033 mmol) and solvent (0.6 mL) were added into an NMR tube along with a sealed glass capillary filled with $(CD_3)_2SO$ as NMR lock signal. The species formed after 16 h at 50 ºC were examined by ^1H NMR and quantified using

1,4-dioxane as an internal standard. The product observed in these reactions, 5-phenyl-1*H*-pyrazole, comes from the *in situ* generation and subsequent decomposition of the diazo compound (Eq. S1).

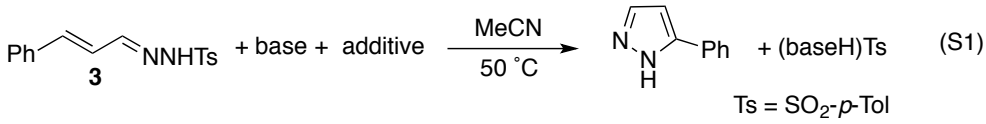

(S1)

Table S1. Decomposition of *N*-tosylhydrazone.

Entry	Hydrazone	Base	Additive	% conversion, 16 h
1	**3**	-	-	0
2	**3**	Na_2CO_3	-	28
3	**3**	Na_2CO_3	$BnEt_3NCl$	100
4	**3**	$(NBu_4)_2CO_3$	-	100
5	**3**	Et_3N	-	100

a) Reaction conditions: **3** (0.033 mmol), base (0.05 mmol), additive (0.033 mmol), solvent (0.6 mL), 50 ºC, 16 h. Conversion was quantified by ^{1}H NMR using 1,4-dioxane as internal standard.

The solubility of the sodium hydrazonates is very low in acetonitrile whereas the ammonium salts are completely soluble. The higher conversion observed in the presence of a trialkylammonium chloride (entry 3) and when a base provides an ammonium counterion (entries 4 and 5) reflects this solubility difference.

The decomposition of *N*-tosylhydrazone **3** in the presence of triethylamine (leading to a soluble ammonium hydrazonate) was monitored by ^{1}H NMR. **3** (0.12 mmol), Et_3N (0.18 mmol) and CD_3CN (0.7 mL) were added into an NMR tube. The formation of the pyrazole was monitored for 4 h at 50 ºC by ^{1}H NMR using 1,4-dioxane as an internal standard. The only product observed in this reaction is 5-phenyl-1*H*-pyrazole (Figure S2) which comes from the *in situ* generation of diazo compound N_2CH-CH=CHPh. The progress of the reaction is shown in Figure S3.

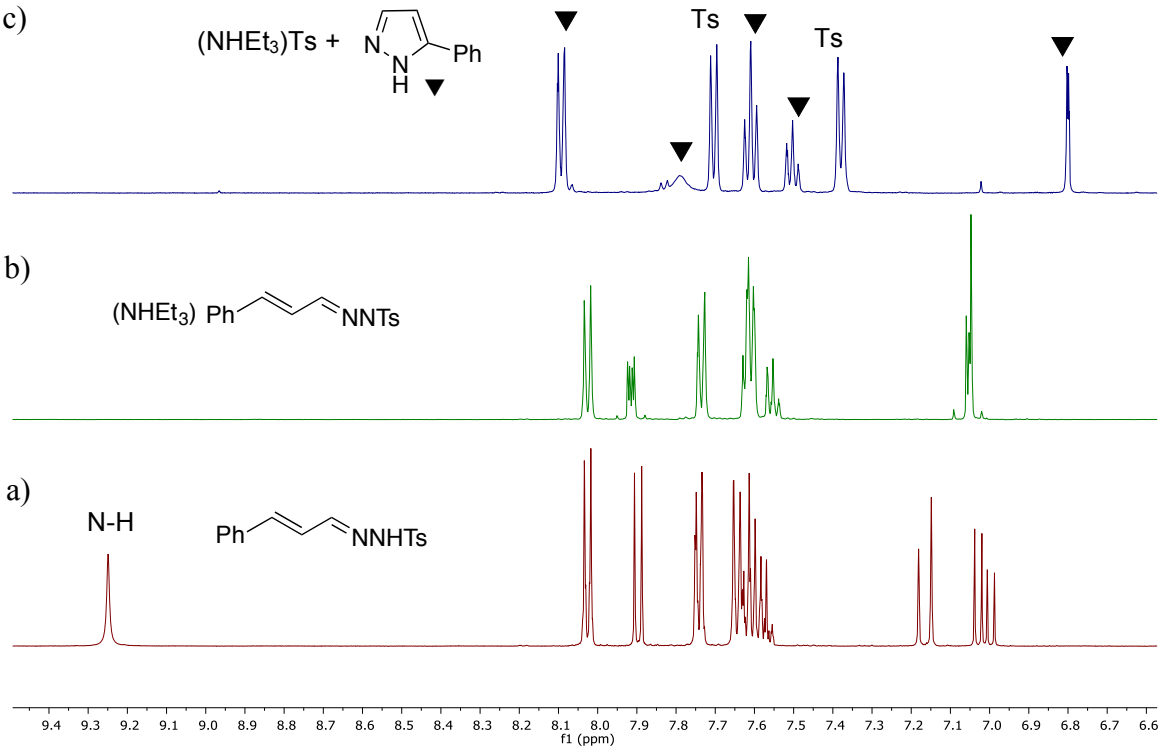

Figure S2. ^{1}H NMR (499.73, MHz, CD_3CN, 298 K) of: a) Hydrazone **3**; b) the ammonium hydrazonate formed upon addition of NEt_3 to sample a; c) sample b after heating at 50 ˚C for 16 h, showing the complete transformation into 5-phenyl-1*H*-pyrazole (Ts = SO_2-*p*-Tol).

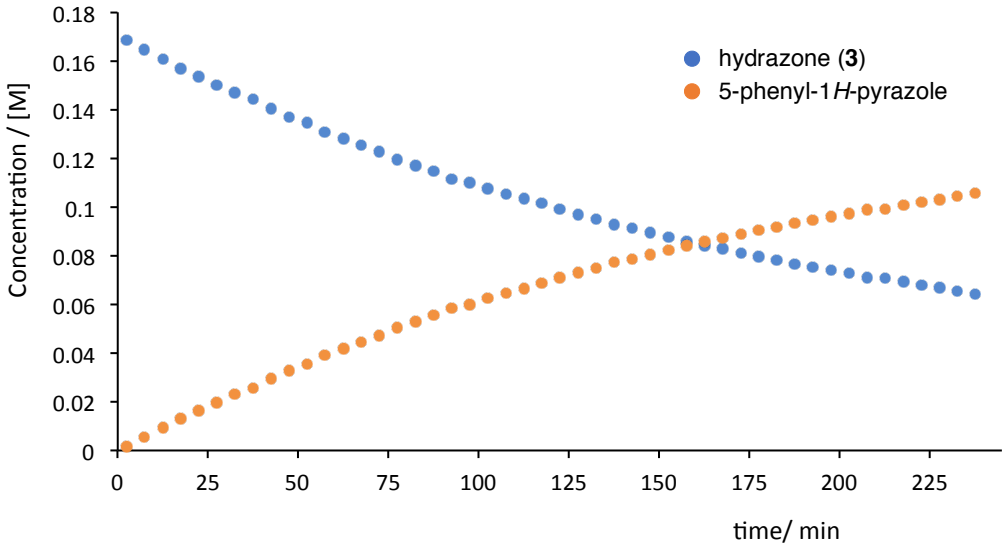

Figure S3. Plot of concentration vs time for the decomposition of *p*-TolSO_2NHNCH-CH=CHPh (**3**) in CD_3CN at 50 ˚C.

1.3- Decomposition of N-tosylhydrazonato palladium complexes.

1.3.1. Decomposition of individual complexes.

[Pd(C_6F_5)(dppe){(*p*-TolSO_2)N-N=CH-CH=CHPh}] (**5a**, 0.006 mmol) was dissolved in CH_3CN (0.6 mL) and the solution was placed in an NMR tube along with a sealed glass capillary filled with $(CD_3)_2SO$ as NMR lock signal. The species formed in solution at the specified temperature and time were examined by ^{19}F and ^{31}P NMR (Eq. S2).

The same result shown in Eq. S2 was obtained when Li_2CO_3 (0.012 mmol) was added to the solution. However, in the presence of the strong base K^tBuO (0.012 mmol) the pyrazolate complex **8** was formed (Eq. S3). The identity of the complexes was determined by comparison with independently prepared samples.

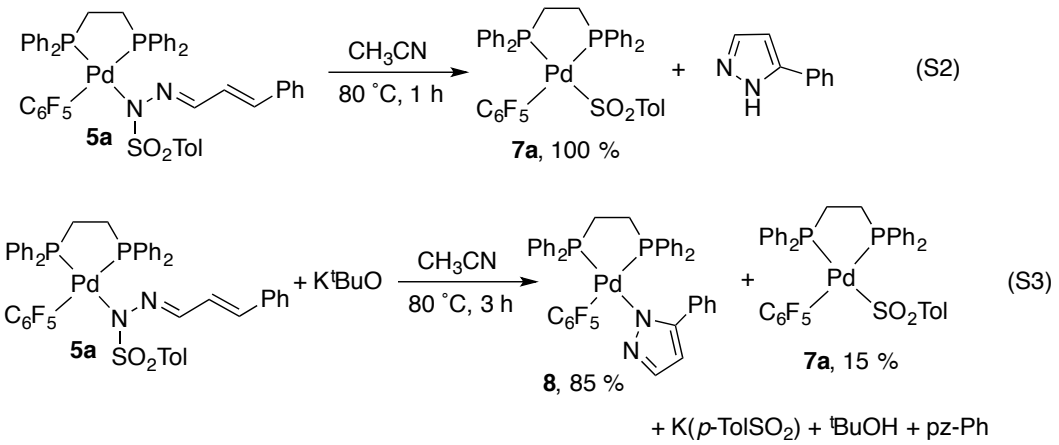

1.3.2 Crossover experiments

*Reaction of [Pd(C_6F_5)(dppe){(p-TolSO_2)N-N=CH-CH=CHPh}] (**5a**) and [Pd(C_6F_5)(dppf){(PhSO_2)N-N=CH-CH=CHPh}] (**5c**).*

Complex **5c** (3.0 mg, 0.0027 mmol), complex **5a** (2.6 mg, 0.0027 mmol) and dry CH_3CN (0.6 mL) were added to a 5 mm NMR tube along with a sealed glass capillary filled with $(CD_3)_2SO$ as NMR lock signal. The species formed in solution at room temperature were examined by ^{31}P and ^{19}F NMR. The resulting mixture was heated at 80 ˚C and checked after 2 h. The same experiment was carried out and monitored by ^{19}F NMR at 50 ºC for 4 h (Figure S7). The species formed were identified by comparison with samples of the complexes prepared independently.

Scheme S1 show the species formed by scrambling of the hydrazonato ligands at room temperature (Figure S4) and of the sulfinate ligands upon decomposition at 80 ˚C (Figures S5 and S6).

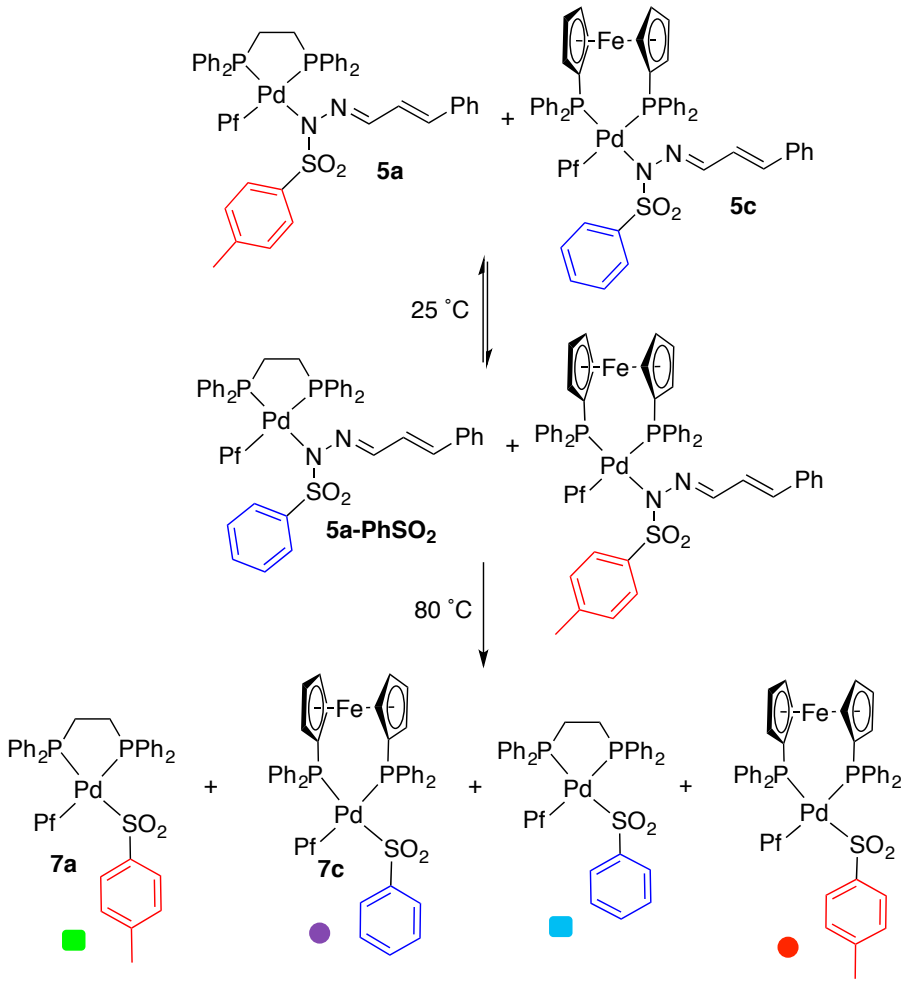

Scheme S1. Crossover experiment between complex **5a** and complex **5c** (Pf = C_6F_5).

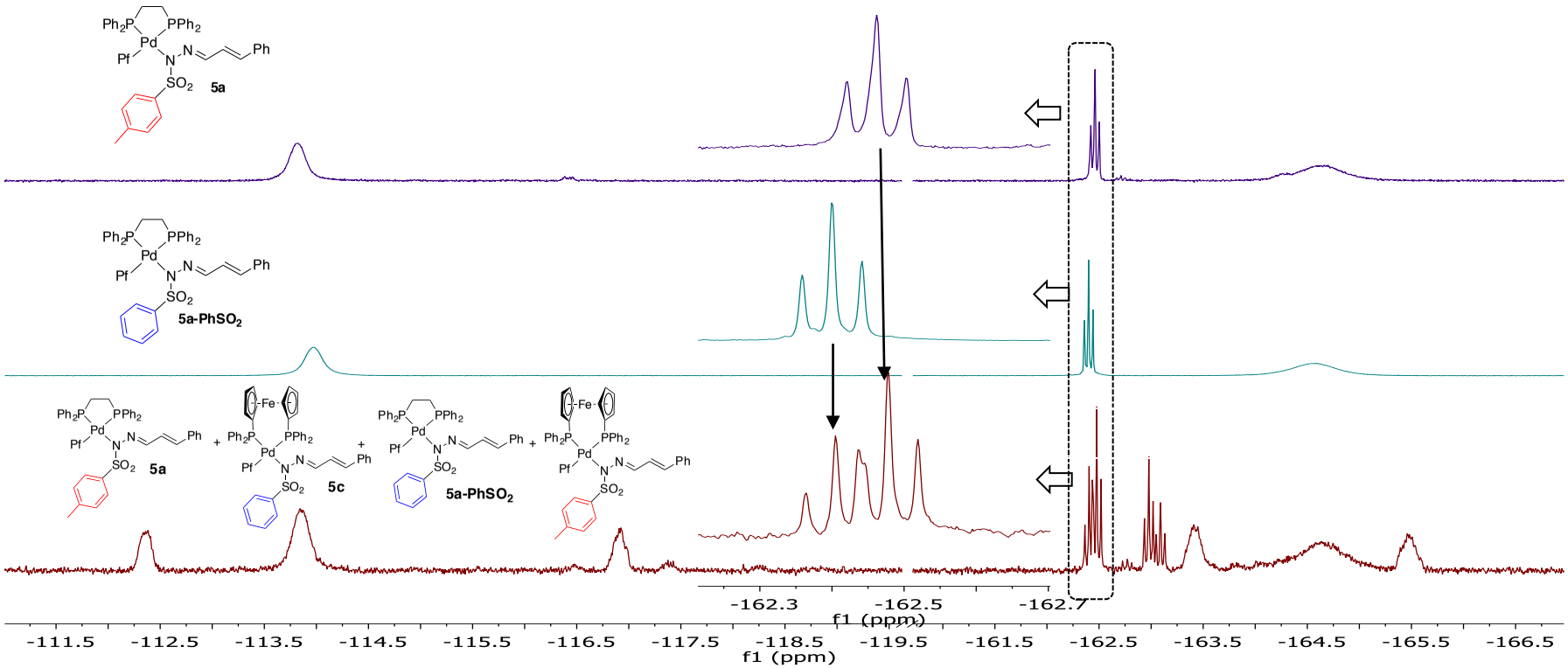

Figure S4. ^{19}F NMR (470.17 MHz, CH_3CN/DMSO-d6 capillary) spectra of: a) The reaction of complexes **5a** and **5c** at room temperature for 30 min, showing the formation of two new species by scrambling of the hydrazonato ligands. These species can be clearly seen in the F_{para} region (the F_{ortho} and F_{meta} signals overlap with the starting complexes). The F_{para} region for the dppe complexes is enlarged and can be compared with the spectra of the N-phenylsulfinyl-hydrazonato complex **5a-SO$_2$Ph** (b) and the *N*-tosylhydrazonato derivative **5a** (c).
■ dppe complexes; ❍ dppf complexes (restricted rotation of the C_6F_5 group leads to inequivalent F_{ortho} and F_{meta} signals). Pf = C_6F_5.

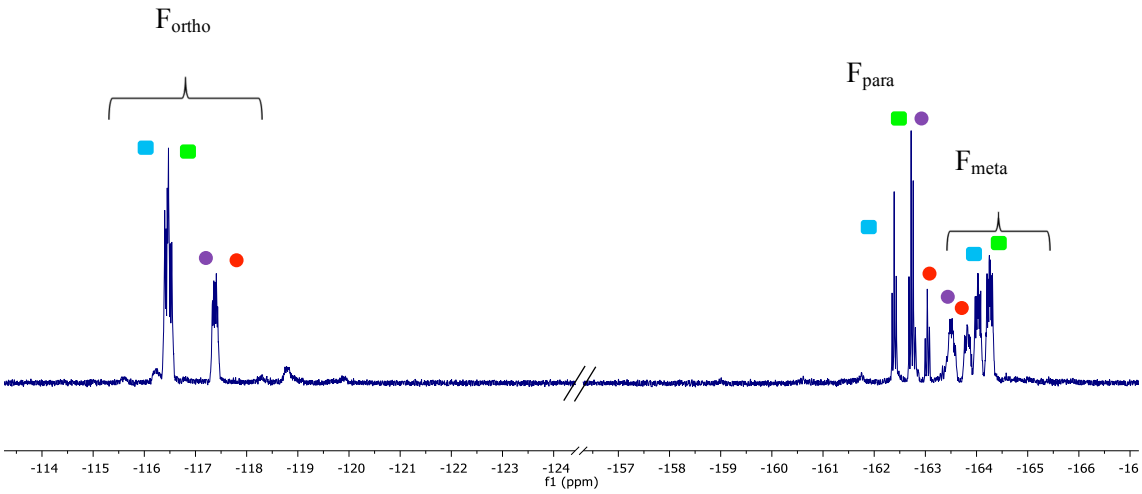

Figure S5. ^{19}F NMR (470.17 MHz, CH_3CN/DMSO-d6 capillary) of the reaction of complexes **5a** and **5c** for 2 h at 80 ºC leading to a mixture of the four possible sulfinato-Pd complexes (for label key, see Scheme S1).

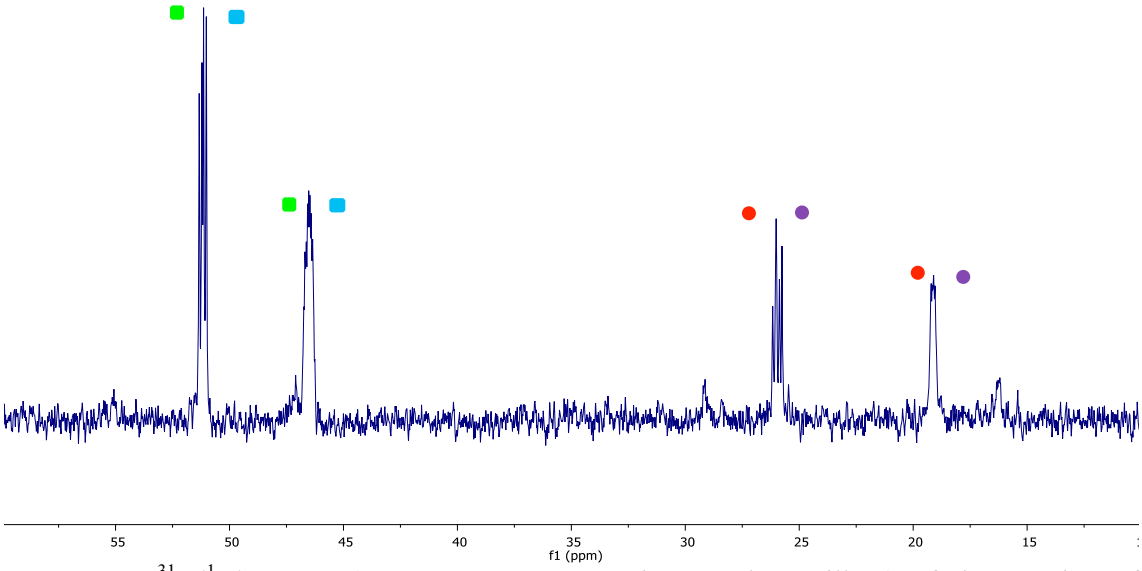

Figure S6. ^{31}P{^{1}H} NMR (202.31, MHz, CH_3CN/DMSO-d6 capillary) of the reaction of complexes **5a** and **5c** for 2 h at 80 ºC leading to a mixture of the four possible sulfinato-Pd complexes (for label key, see Scheme S1)

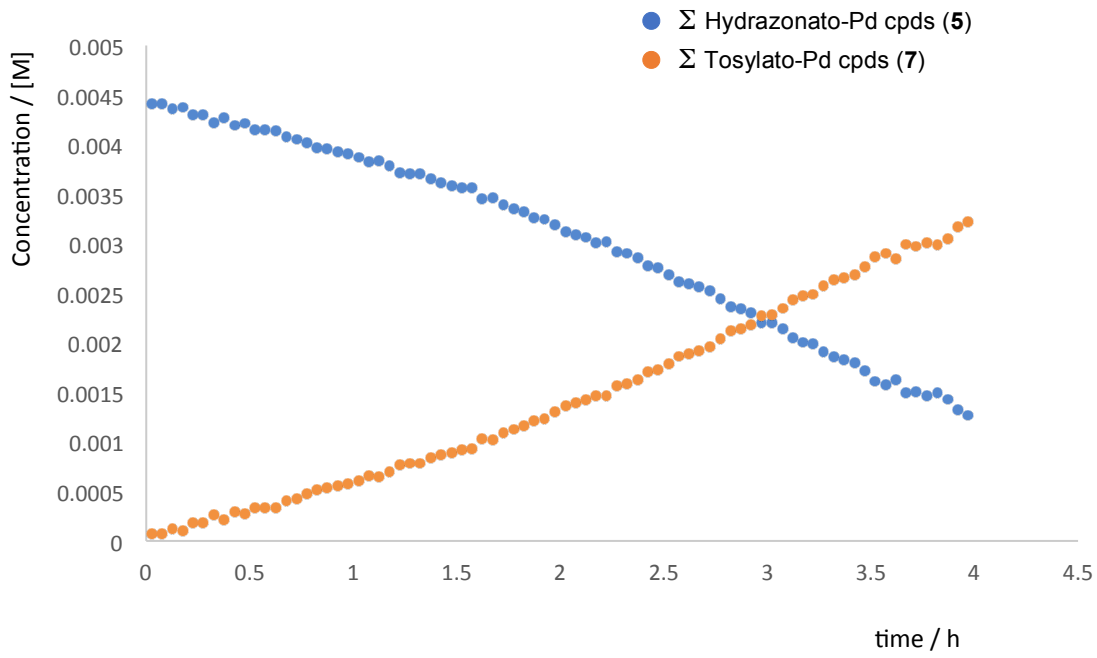

Figure S7. Plot of concentration vs time for the decomposition of the mixture of hidrazonato complexes to give a mixture of arylsulfinato derivatives as shown in Scheme S1. Reaction conditions: MeCN, 50 ˚C.

*Reaction of [Pd(C_6F_5)(dppe)(p-TolSO_2)] (7**a**) and [Pd(C_6F_5)(dppf)(PhSO_2)] (7**c**).*

Complex **7a** (2.2 mg, 0.0027 mmol), complex **7c** (2.6 mg, 0.0027 mmol) and dry CH_3CN (0.6 mL) were added to a 5 mm NMR tube along with a sealed glass capillary filled with $(CD_3)_2SO$ as NMR lock signal. The species formed in solution at room temperature were examined by ^{31}P and ^{19}F NMR (Figure S8)

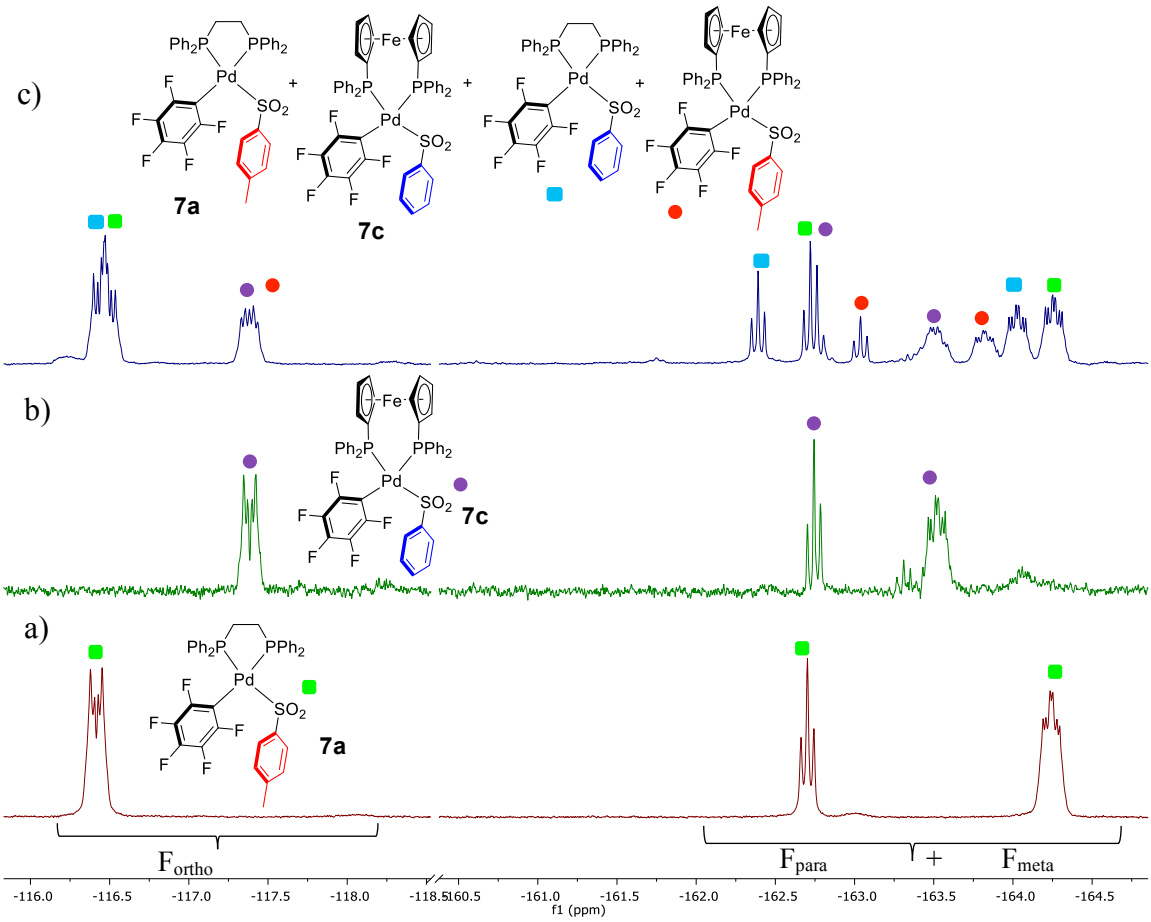

Figure S8. ^{19}F NMR (470.17 MHz, δ, $CH_3CN/(CD_3)_2SO$ capillary) at 298 K of: a) complex **7a**; b) complex **7c**; c) a mixture of **7a** and **7c** showing the scrambling of the sulfinate groups.

1.4- Ligand substitution reactions with diazocompounds.

Table S2. Products of the reaction of diazoalkane N_2=CH-CH=CHPh with palladium complexes **1**, **2**, **5** and **7** (Pf = C_6F_5; Ts SO_2-*p*-Tol)).[a]

Entry	[Pd]	Products (%)[b]
1	[Pd(Pf)(Br)(dppe)] (**1a**)	**9a** (10)[c]
2	[Pd(Ph)(Br)(dppe)] (**1b**)	**9b** (100)
4	[Pd(Pf)(NCMe)(dppe)]BF_4 (**2a**)	**9a** (100)
5	[Pd(Ph)(NCMe)(dppe)]BF_4 (**2b**)	**9b** (100)
7	[Pd(Pf)(Ts)N-N=CH-CH=CHPh)(dppe)] (**5a**)	**9a** (10), **7a** (5), **8** (6)[c]
8	[Pd(Ph)Ts N-N=CH-CH=CHPh)(dppe)] (**5b**)	**9b** (100)
9	[Pd(Pf)(SO_2-*p*-Tol)(dppe)] (**7a**)	**9a** (15)[c]
10	[Pd(Ph)(SO_2-*p*-Tol)(dppe)] (**7b**)	**9b** (100)

a) Reaction conditions: MeCN as solvent at 298 K for 10 min. b) The new species formed were determined by ^{19}F NMR and ^{31}P NMR. c) Unreacted starting material accounts for the remaining percentage.

2. Data for X-ray molecular structures.

Table S3. Crystal data and structure refinement parameters for **5c**, **6**, **7a** and **7c**.

Compound number	**7a**	**7c**	**6**	**5c**
Empirical formula	$C_{40}H_{33}Cl_2F_5O_2P_2PdS$	$C_{46}H_{33}F_5FeO_2P_2PdS$	$C_{92}H_{74}F_{10}N_4O_4P_4Pd_2S_2$	$C_{55}H_{41}F_5FeN_2O_2P_2PdS$
Formula weight	911.96	968.97	1890.35	1113.15
Temperature/K	298	298	298(2)	298
Crystal system	monoclinic	monoclinic	triclinic	orthorhombic
Space group	C2/c	$P2_1/n$	P-1	$Pca2_1$
a/Å	22.5623(15)	12.9070(6)	12.9823(5)	23.4624(8)
b/Å	11.1264(8)	10.8331(5)	14.2919(5)	10.2943(3)
c/Å	31.1487(13)	31.6024(13)	26.8298(11)	20.1369(6)
α/°	90	90	88.413(3)	90
β/°	94.857(4)	100.506(5)	89.913(3)	90
γ/°	90	90	73.042(3)	90
Volume/$Å^3$	7791.4(8)	4344.7(3)	4759.6(3)	4863.7(3)
Z	8	4	2	4
ρ_{calc}g/cm^3	1.555	1.481	1.319	1.520
μ/mm^{-1}	0.808	0.927	0.557	0.841
F(000)	3680.0	1952.0	1920.0	2256.0
Crystal size/mm^3	0.28 × 0.11 × 0.064	0.398 × 0.21 × 0.128	0.176 × 0.134 × 0.079	0.295 × 0.197 × 0.104
Radiation	MoKα (λ = 0.71073)	MoKα (λ = 0.71073)	MoKα (λ = 0.71073)	Mo Kα (λ = 0.71073)
2Θ range for data collection/°	6.628 to 59.22	6.754 to 59.568	3.384 to 50.054	5.264 to 59.516
Index ranges	$-30 \le h \le 31$, $-14 \le k \le 15$, $-43 \le l \le 24$	$-17 \le h \le 17$, $-14 \le k \le 11$, $-32 \le l \le 43$	$-15 \le h \le 14$, $-15 \le k \le 17$, $-30 \le l \le 31$	$-25 \le h \le 29$, $-12 \le k \le 14$, $-23 \le l \le 27$
Reflections collected	20606	19107	32504	36962
Independent reflections	9211 [R_{int} = 0.0635, R_{sigma} = 0.1199]	10169 [R_{int} = 0.0309, R_{sigma} = 0.0545]	16805 [R_{int} = 0.0675, R_{sigma} = 0.1451]	10888 [R_{int} = 0.0428, R_{sigma} = 0.0487]
Data/restraints/parameters	9211/0/479	10169/0/523	16805/0/1065	10888/1/622
Goodness-of-fit on F^2	1.045	1.024	0.946	1.054
Final R indexes [I>=2σ (I)]	R_1 = 0.0904, wR_2 = 0.1749	R_1 = 0.0417, wR_2 = 0.0778	R_1 = 0.0646, wR_2 = 0.0967	R_1 = 0.0356, wR_2 = 0.0589
Final R indexes [all data]	R_1 = 0.1820, wR_2 = 0.2111	R_1 = 0.0688, wR_2 = 0.0907	R_1 = 0.1515, wR_2 = 0.1261	R_1 = 0.0575, wR_2 = 0.0686
Largest diff. peak/hole / e $Å^{-3}$	0.61/-0.69	0.43/-0.52	0.47/-0.33	0.42/-0.62

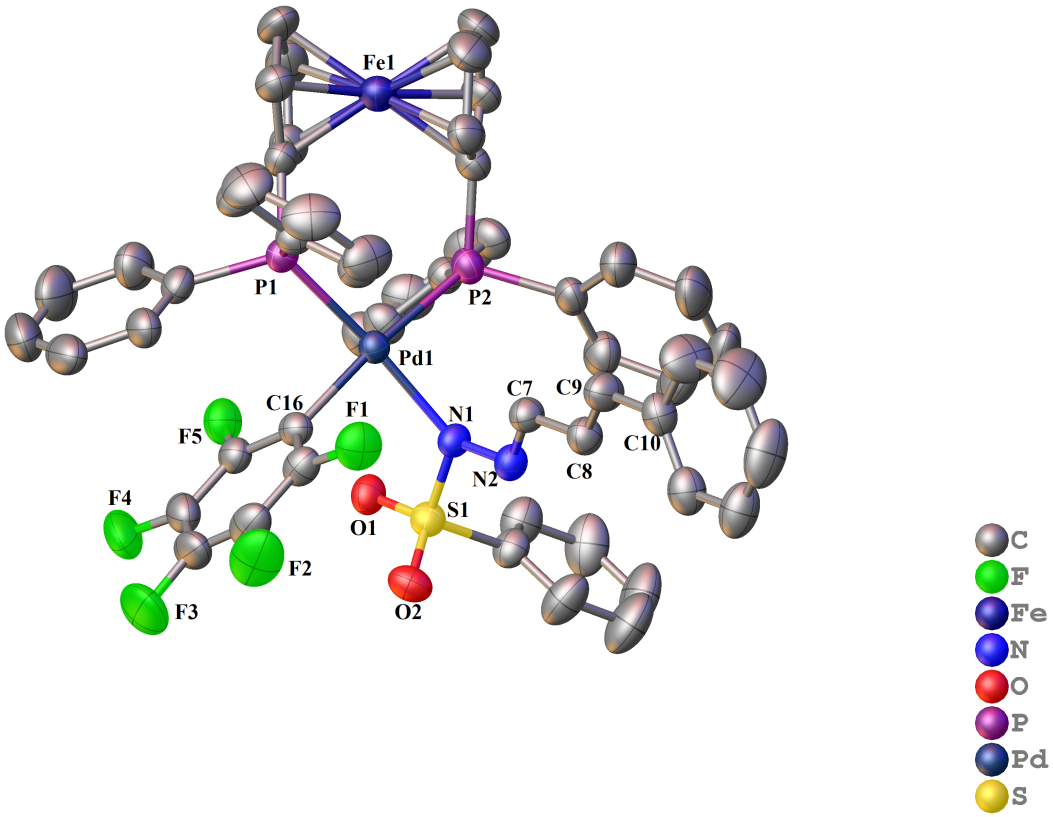

Figure S9. X-ray molecular structure of **5c** (ORTEP 40% probability ellipsoids). Hydrogen atoms are omitted for clarity.

Table S4. Selected bond lengths [Å] and angles [º] for complex **5c** (for numbering scheme see Figure S9).

Pd(1)-P(1)	2.3011(12)	N(2)-C(7)	1.282(5)
Pd(1)-P(2)	2.3698(12)	C(7)-C(8)	1.430(6)
Pd(1)-N(1)	2.109(4)	C(8)-C(9)	1.338(6)
Pd(1)-C(16)	2.047(4)	C(9)-C(10)	1.463(6)
N(1)-N(2)	1.380(5)		
P(1)-Pd(1)-P(2)	101.17(4)	C(16)-Pd(1)-N(1)	87.66(16)

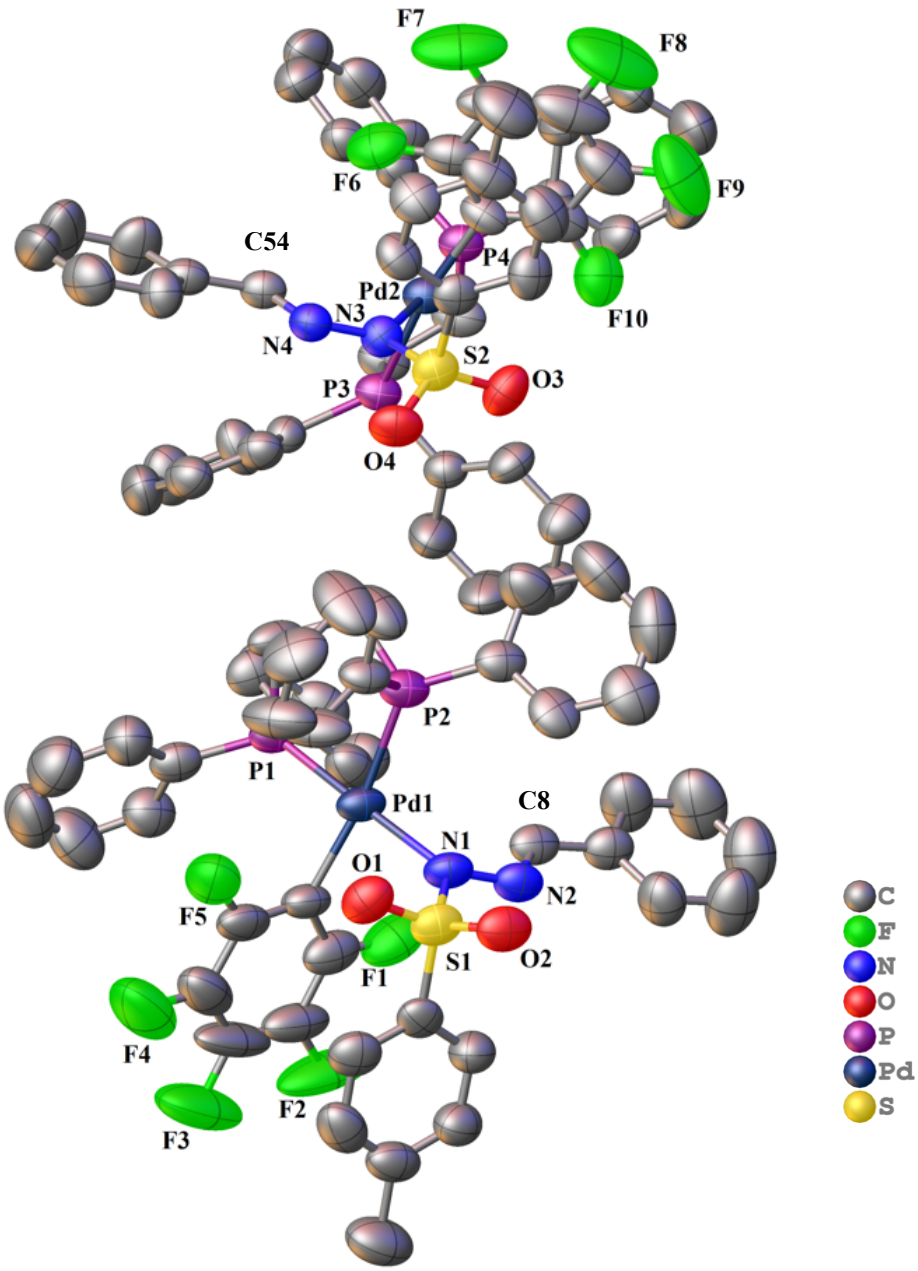

Figure S10. X-ray molecular structure of **6** (ORTEP 40% probability ellipsoids). The two independent molecules found in the unit cell are shown. Hydrogen atoms are omitted for clarity.

Table S5. Selected bond lengths [Å] and angles [º] for complex **6** (for numbering scheme see Figure S10).

Pd(1)-P(1)	2.2461(16)	Pd(2)-P(3)	2.3281(18)
Pd(1)-P(2)	2.3317(18)	Pd(2)-P(4)	2.2502(16)
Pd(1)-N(1)	2.105(5)	Pd(2)-N(3)	2.120(4)
Pd(1)-C(15)	2.045(7)	Pd(2)-C(73)	2.051(6)
N(2)-N(1)	1.382(6)	N(3)-N(4)	1.366(6)
N(2)-C(8)	1.270(7)	N(4)-C(54)	1.290(6)
P(1)-Pd(1)-P(2)	84.56(6)	P(4)-Pd(2)-P(3)	84.49(6)
C(15)-Pd(1)-N(1)	88.8(2)	C(73)-Pd(2)-N(3)	89.4(2)

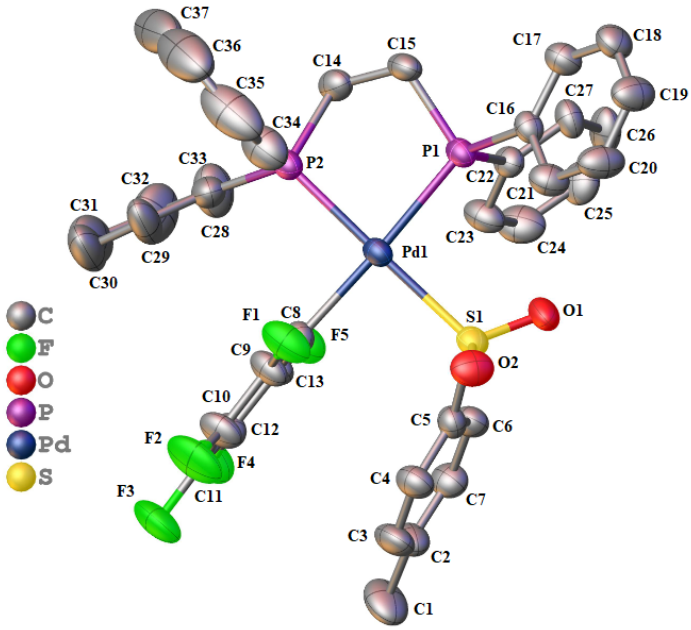

Figure S11. X-ray molecular structure of **7a** (ORTEP 40% probability ellipsoids). Hydrogen atoms and the solvent molecule of CH_2Cl_2 are omitted for clarity

Table S6. Selected bond lengths [Å] and angles [º] for complex **7a** (for numbering scheme see Figure S11).

Pd(1)-P(1)	2.3203(19)
Pd(1)-S(1)	2.337(2)
Pd(1)-P(2)	2.278(2)
Pd(1)-C(8)	2.058(7)
P(2)-Pd(1)-P(1)	84.68(8)
C(8)-Pd(1)-S(1)	89.3(2)

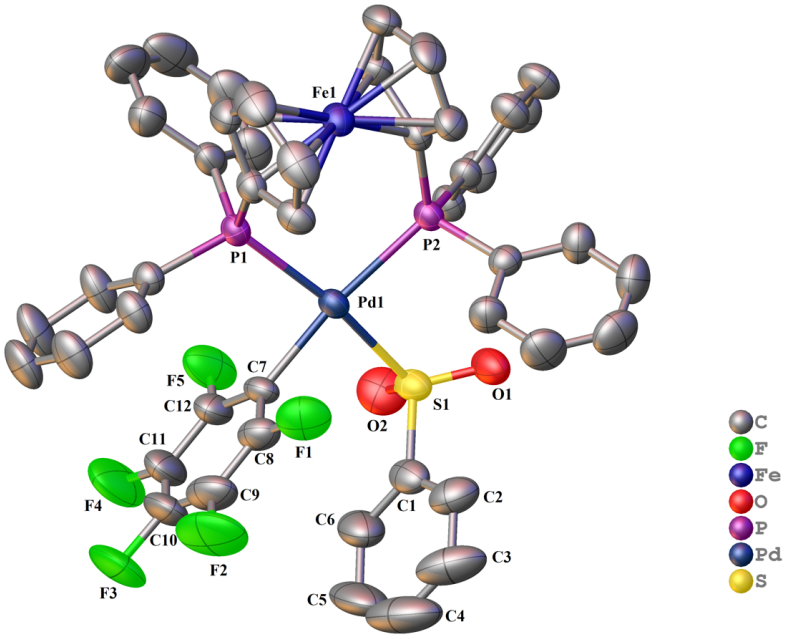

Figure S12. X-ray molecular structure of **7c** (ORTEP 40% probability ellipsoids). Hydrogen atoms are omitted for clarity.

Table S7. Selected bond lengths [Å] and angles [º] for complex **7c** (for numbering scheme see Figure S12).

Pd(1)-P(2)	2.3611(8)
Pd(1)-P(1)	2.3427(8)
Pd(1)-S(1)	2.3656(8)
Pd(1)-C(7)	2.038(3)
P(1)-Pd(1)-P(2)	97.65(3)
C(7)-Pd(1)-S(1)	85.68(8)

3. Selected spectra

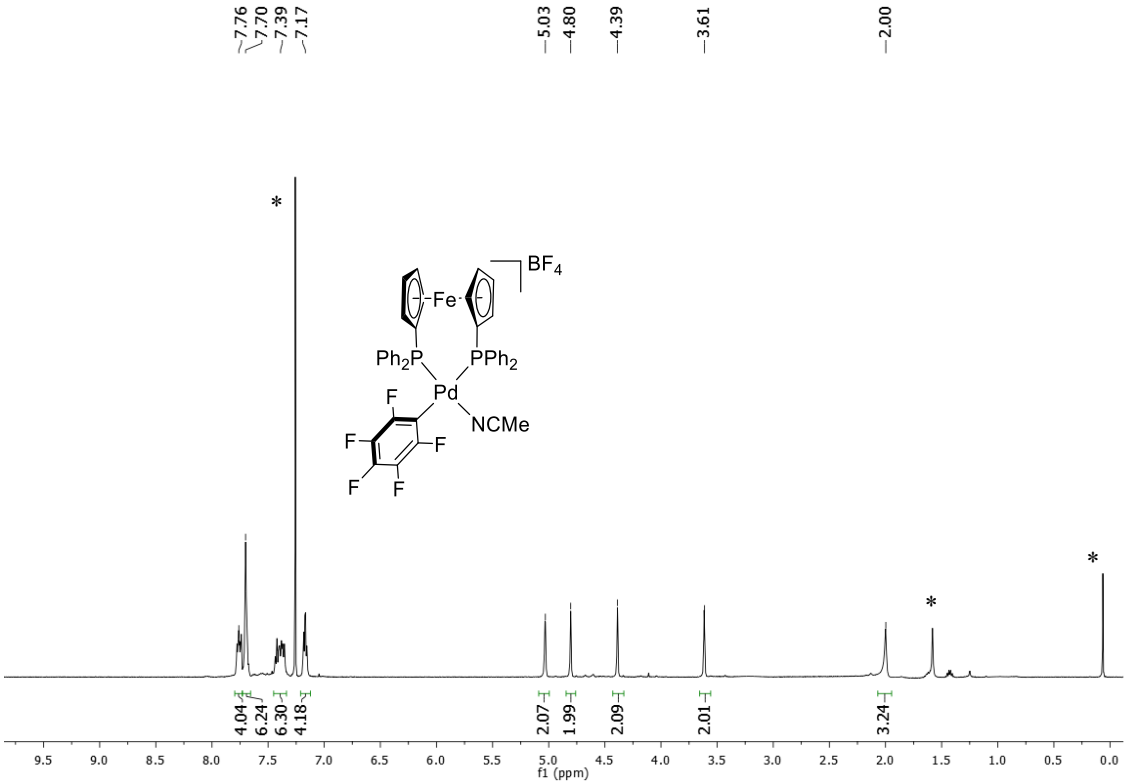

Figure S13. ^{1}H NMR (499.72, MHz, $CDCl_3$) of **[**Pd(C_6F_5)(dppf)($NCCH_3$)](BF$_4$) (**2c**) at 298 K. * Signals corresponding to the solvent (H_2O, chloroform and residual silicone grease).

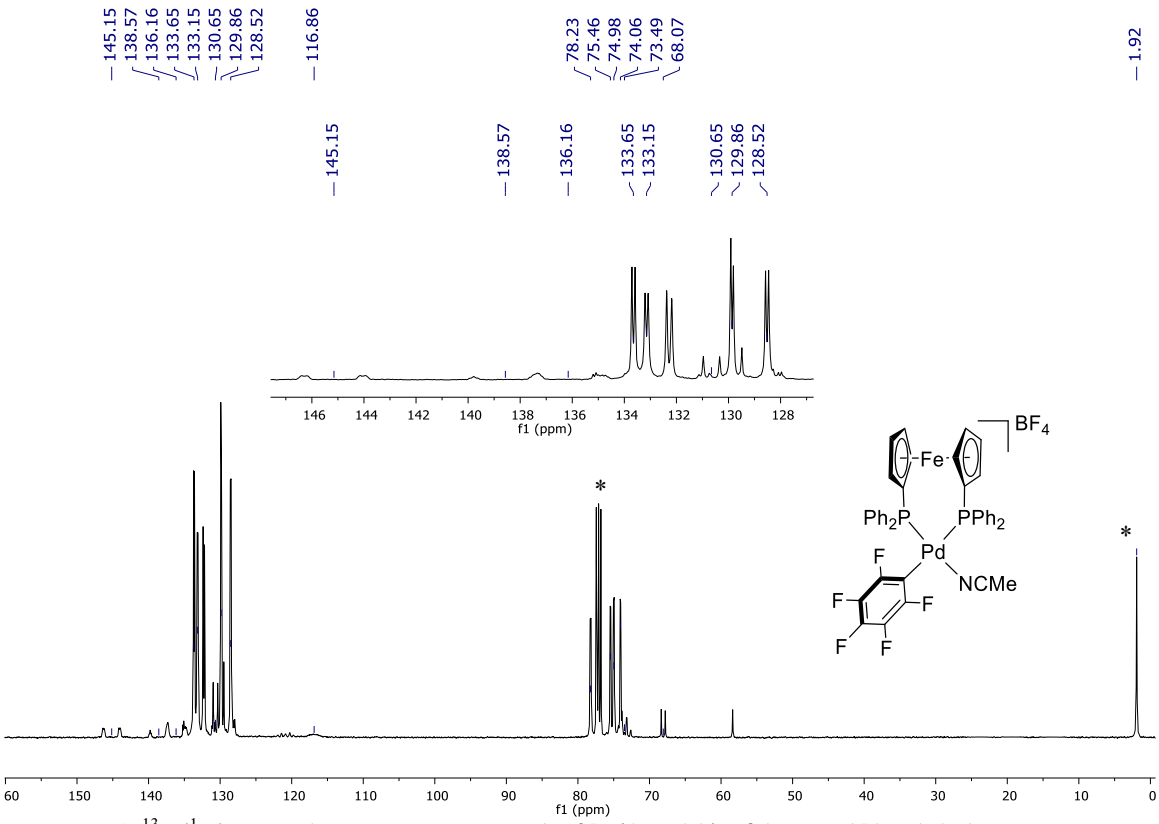

Figure S14. ^{13}C{^{1}H} NMR (125.67 MHz, CD_3CN) of [Pd(C_6F_5)(dppf)($NCCH_3$)](BF$_4$) (**2c**) at 298 K.
* Signals corresponding to the solvent (chloroform and residual silicone grease).

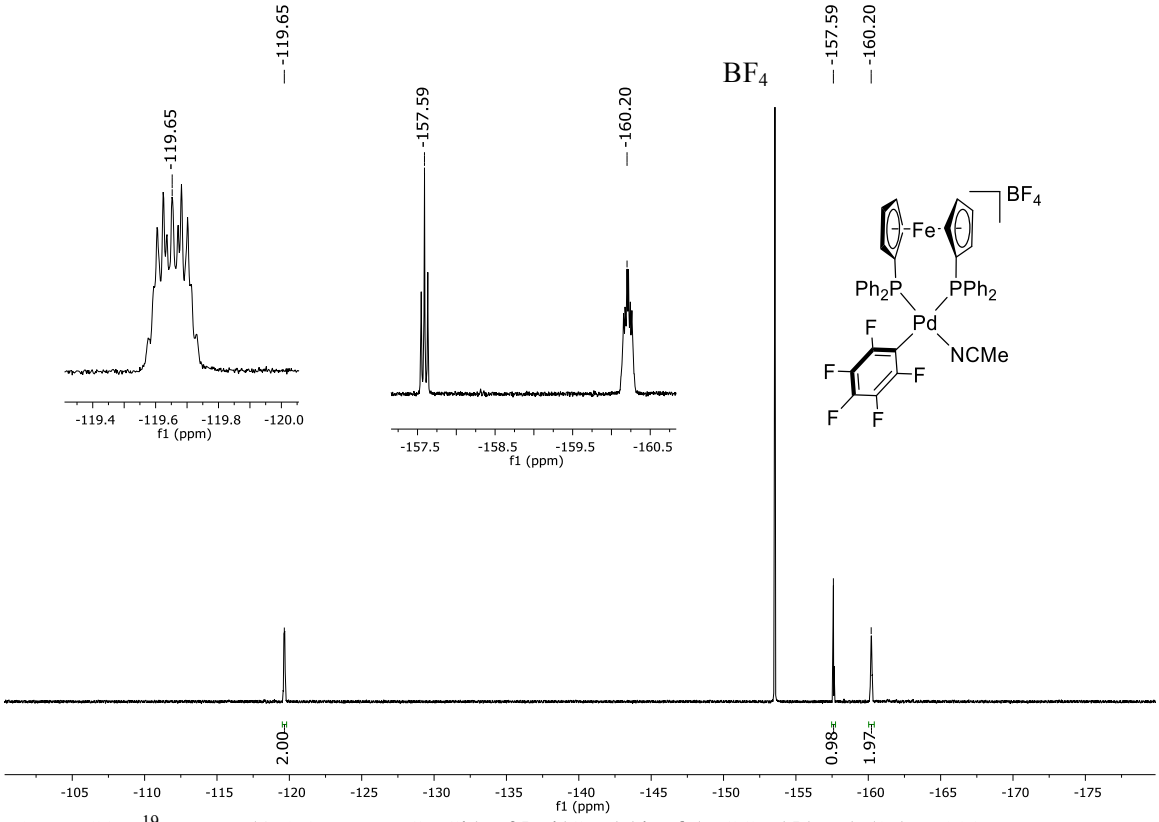

Figure S15. ^{19}F NMR (470.17 MHz, $CDCl_3$) of $[Pd(C_6F_5)(dppf)(NCCH_3)](BF_4)$ (**2c**) at 298 K.

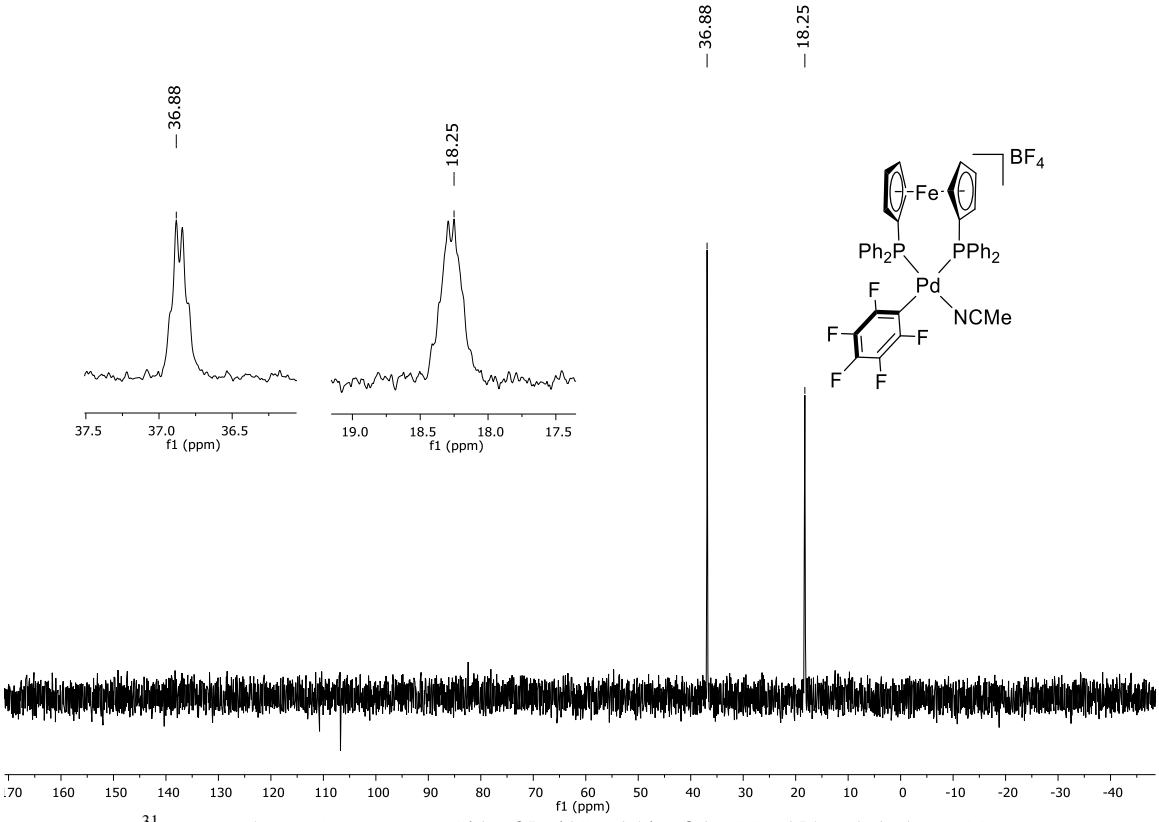

Figure S16. ^{31}P NMR (202.31, MHz, $CDCl_3$) of $[Pd(C_6F_5)(dppf)(NCCH_3)](BF_4)$ (**2c**) at 298 K.

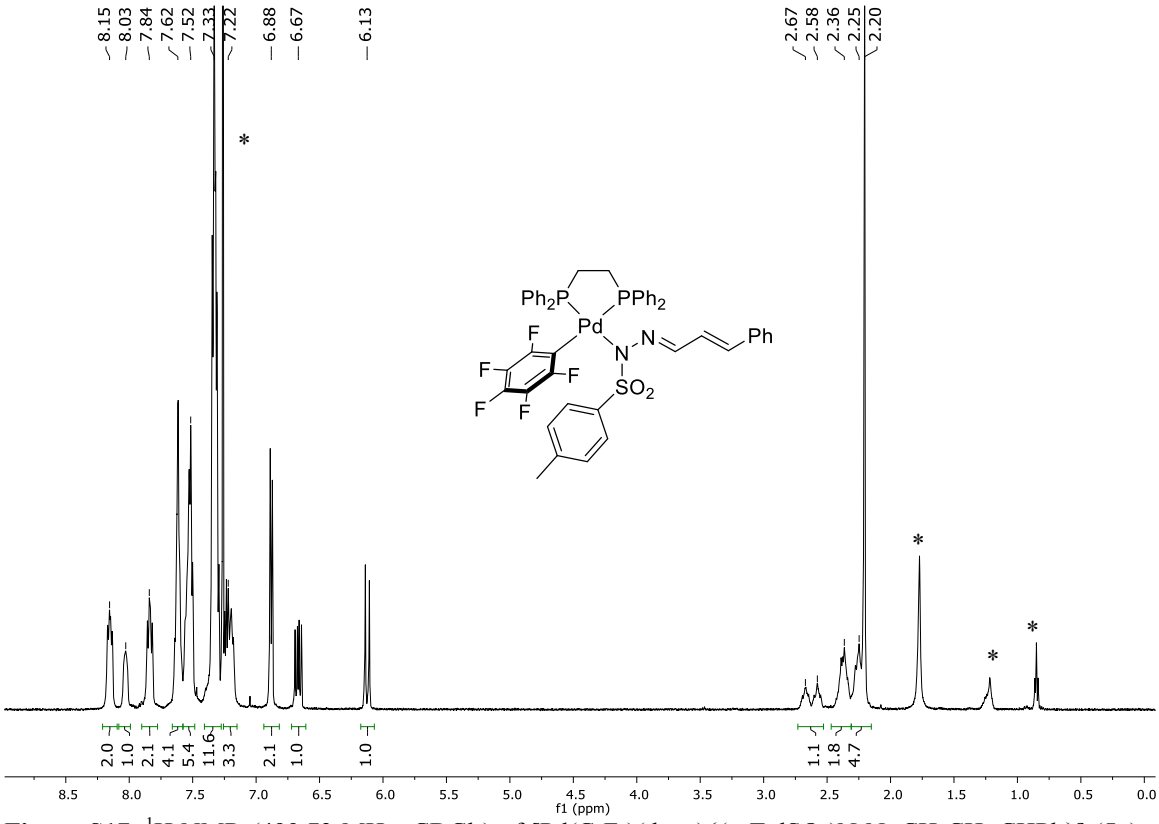

Figure S17. ^{1}H NMR (499.73 MHz, $CDCl_3$) of [Pd(C_6F_5)(dppe){(*p*-TolSO_2)N-N=CH-CH=CHPh}] (**5a**) at 233 K. * Signals corresponding to the solvent (H_2O, chloroform and traces of hexanes).

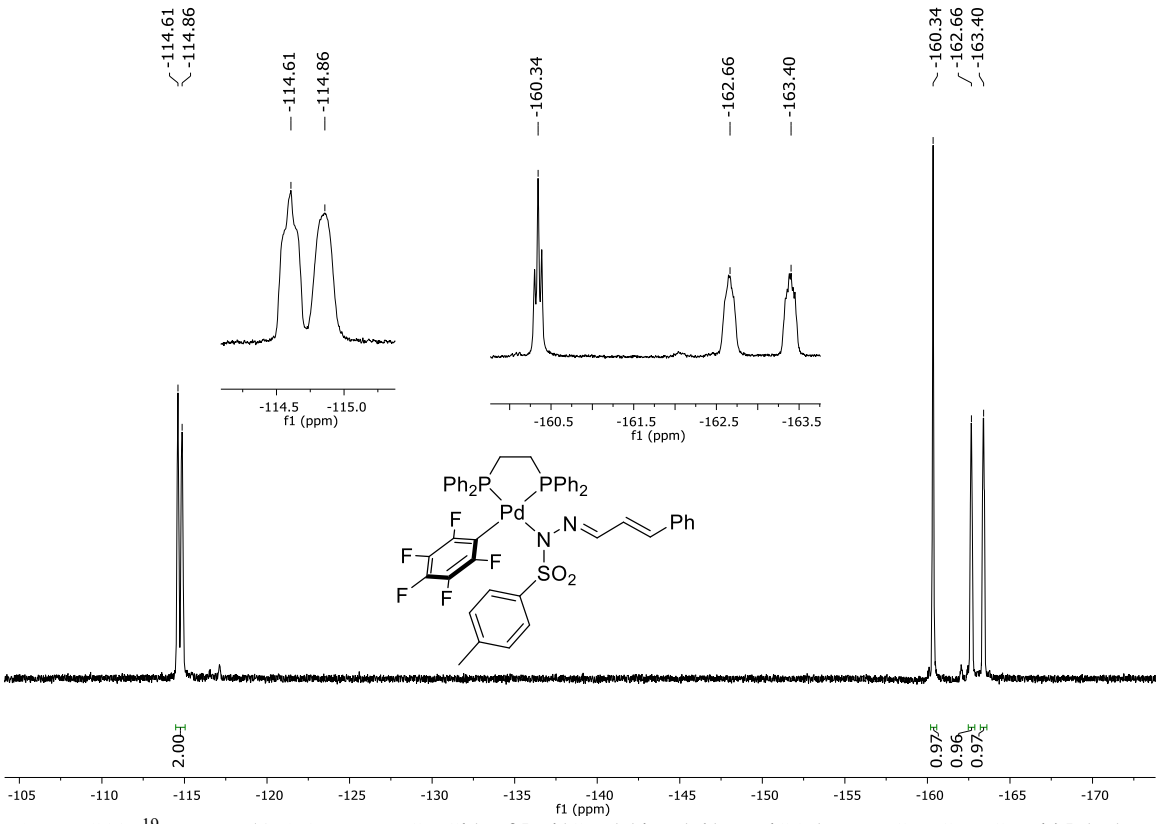

Figure S18. ^{19}F NMR (470.17 MHz, $CDCl_3$) of [Pd(C_6F_5)(dppe){(*p*-TolSO_2)N-N=CH-CH=CHPh}] (**5a**) at 233 K.

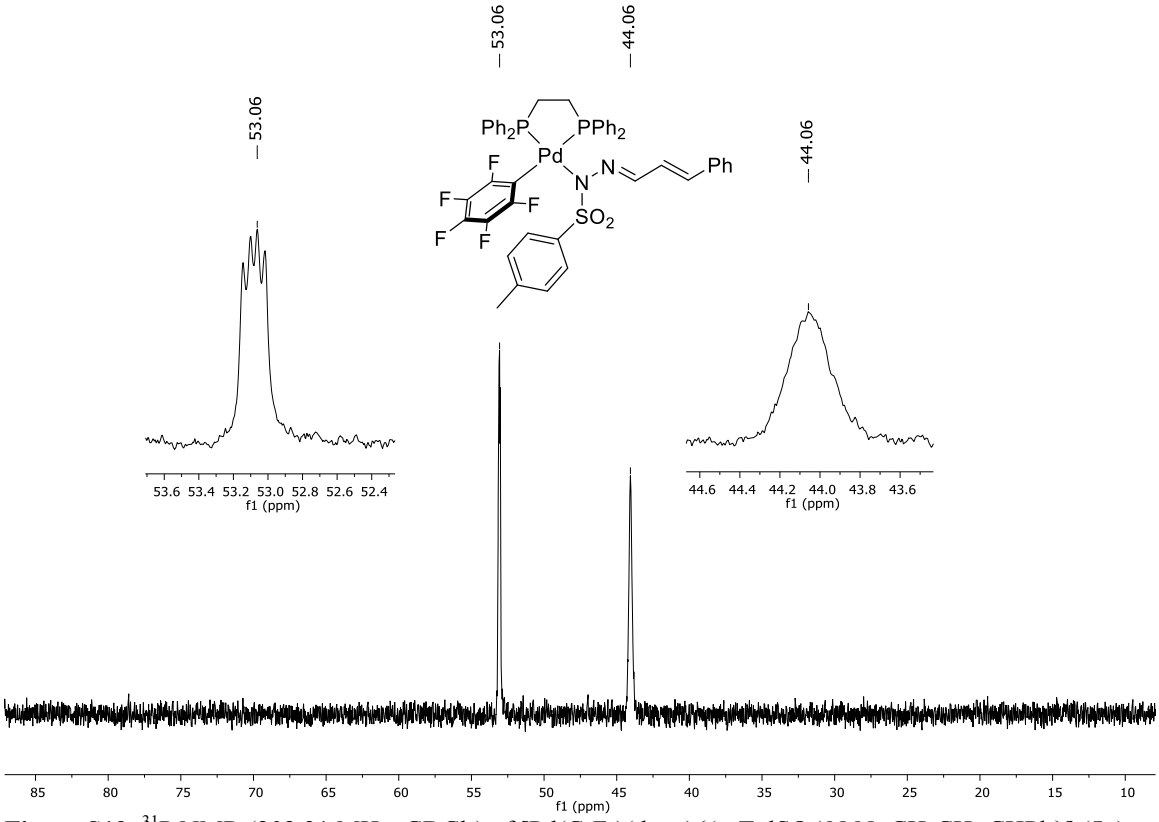

Figure S19. ^{31}P NMR (202.31 MHz, $CDCl_3$) of [Pd(C_6F_5)(dppe){(*p*-TolSO_2)N-N=CH-CH=CHPh}] (**5a**) at 233 K.

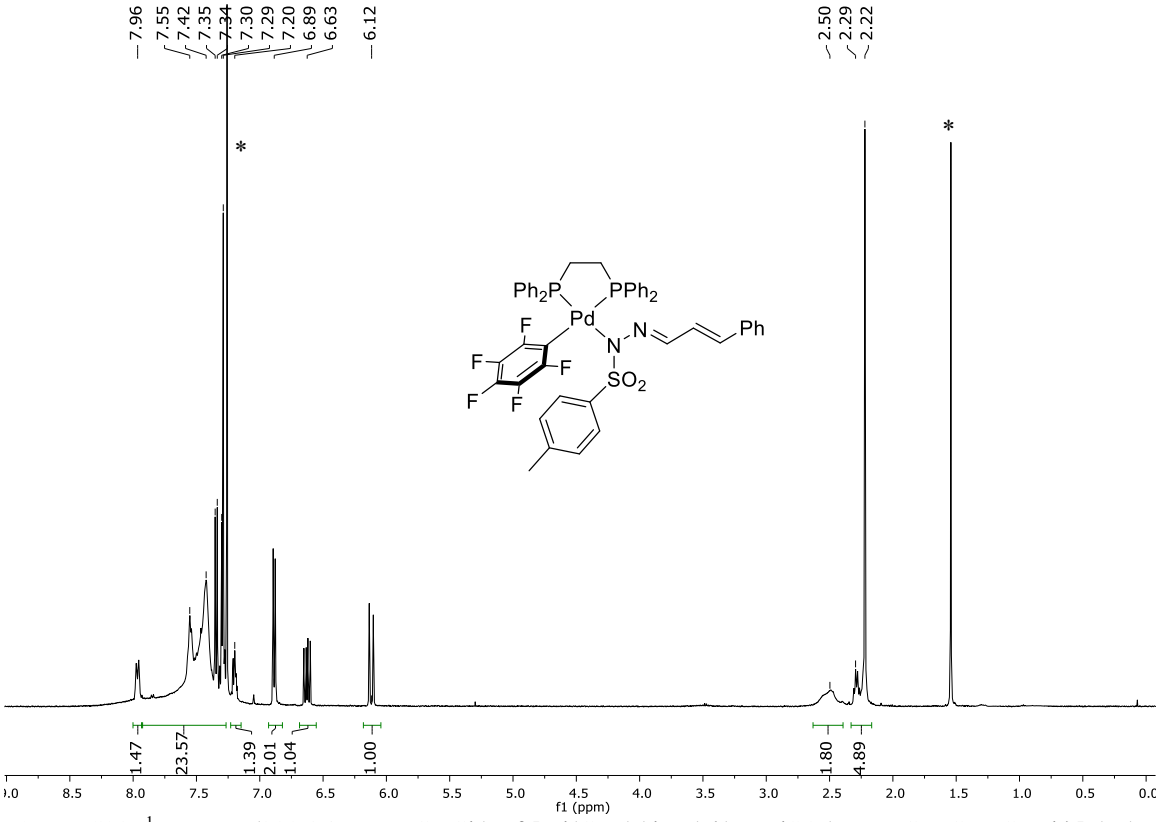

Figure S20. ^{1}H NMR (399.86 MHz, $CDCl_3$) of [Pd(C_6F_5)(dppe){(*p*-TolSO_2)N-N=CH-CH=CHPh}] (**5a**) at 298 K. * Signals corresponding to the solvent (H_2O and chloroform).

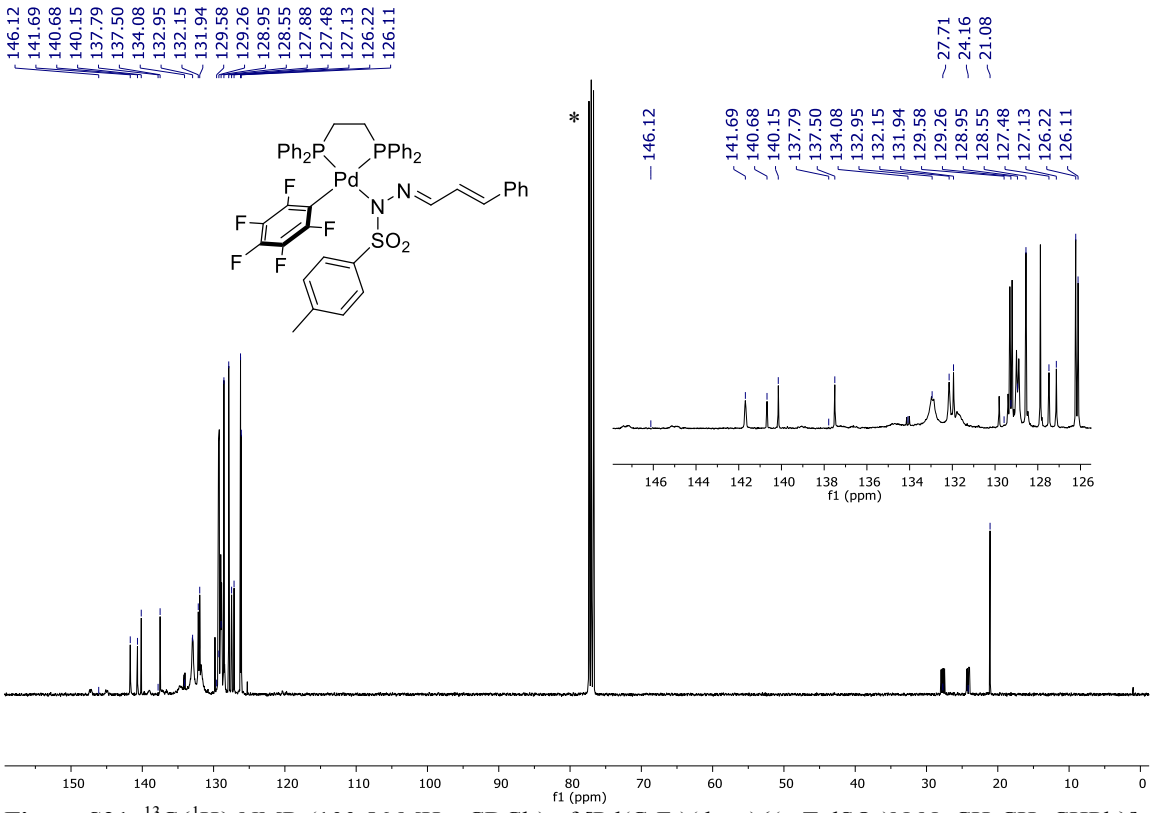

Figure S21. $^{13}C\{^{1}H\}$ NMR (100.56 MHz, $CDCl_3$) of [Pd(C_6F_5)(dppe){(*p*-TolSO_2)N-N=CH-CH=CHPh}] (**5a**) at 298 K. * Signals corresponding to the solvent (chloroform).

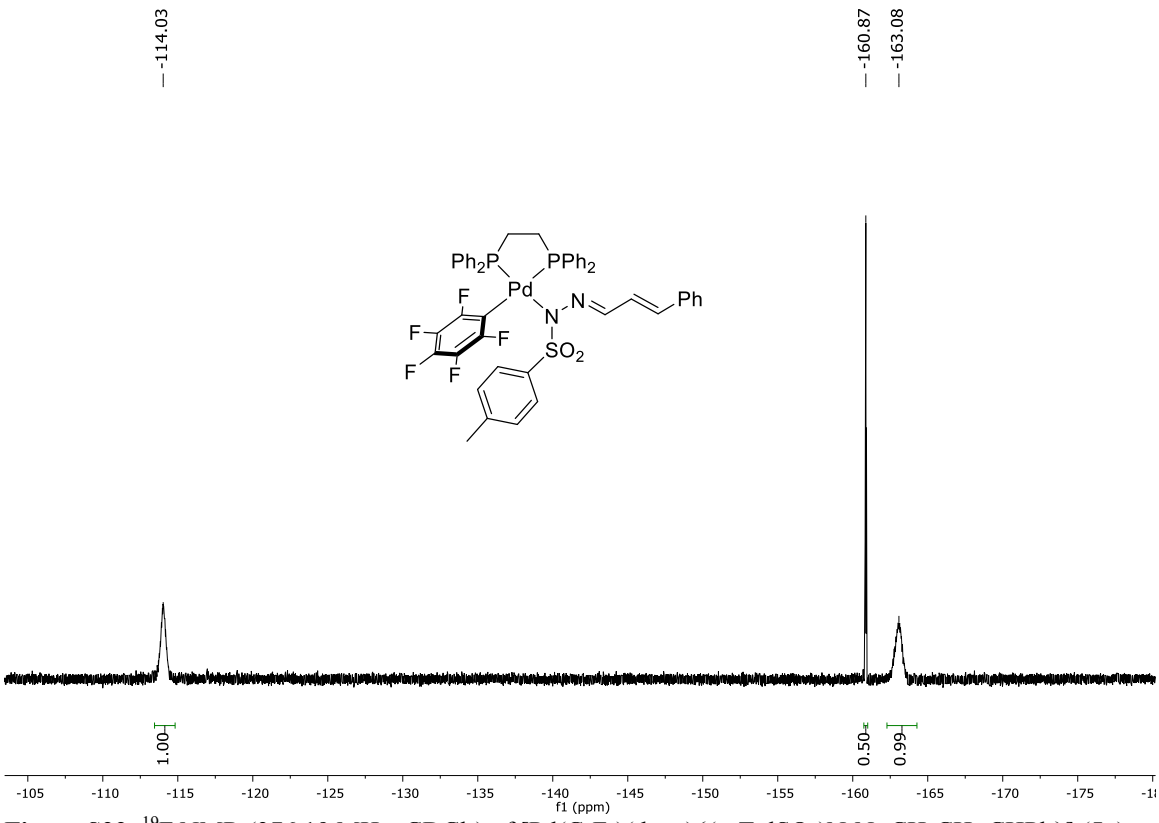

Figure S22. ^{19}F NMR (376.19 MHz, $CDCl_3$) of [Pd(C_6F_5)(dppe){(*p*-TolSO_2)N-N=CH-CH=CHPh}] (**5a**) at 298 K.

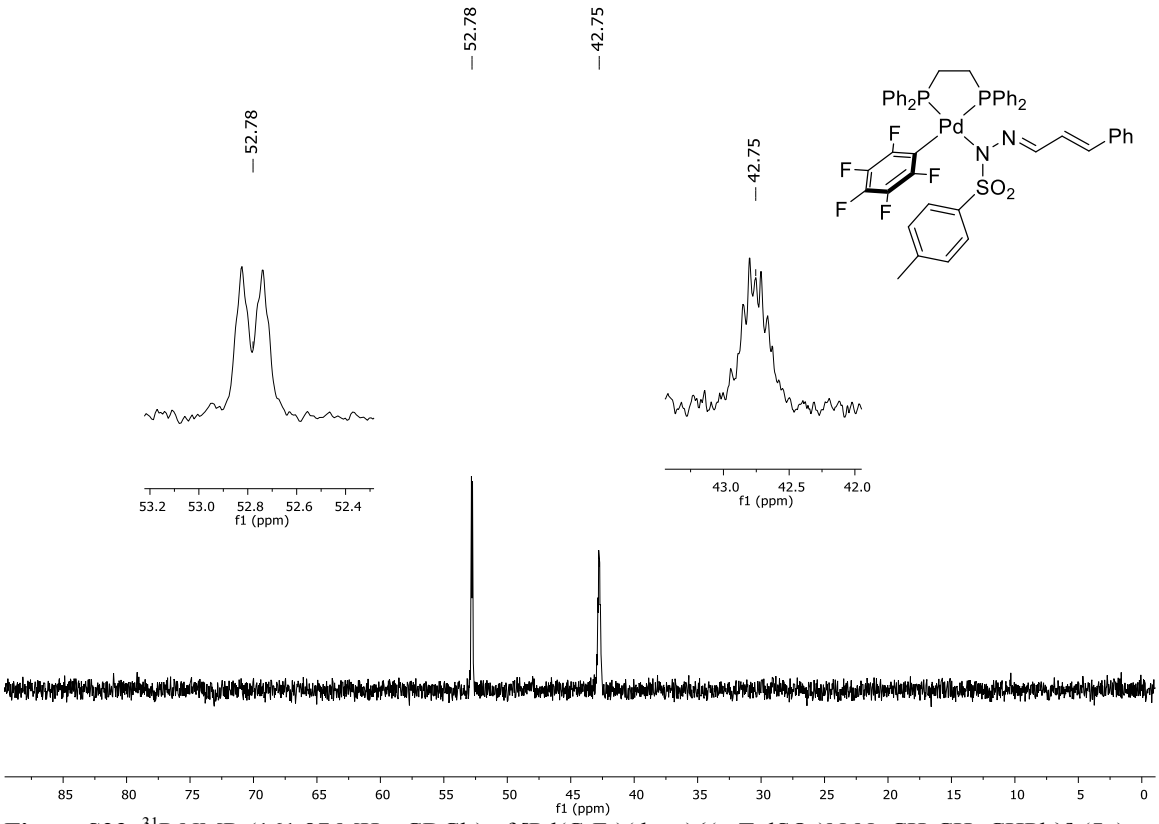

Figure S23. ^{31}P NMR (161.87 MHz, $CDCl_3$) of [Pd(C_6F_5)(dppe){(*p*-TolSO_2)N-N=CH-CH=CHPh}] (**5a**) at 298 K.

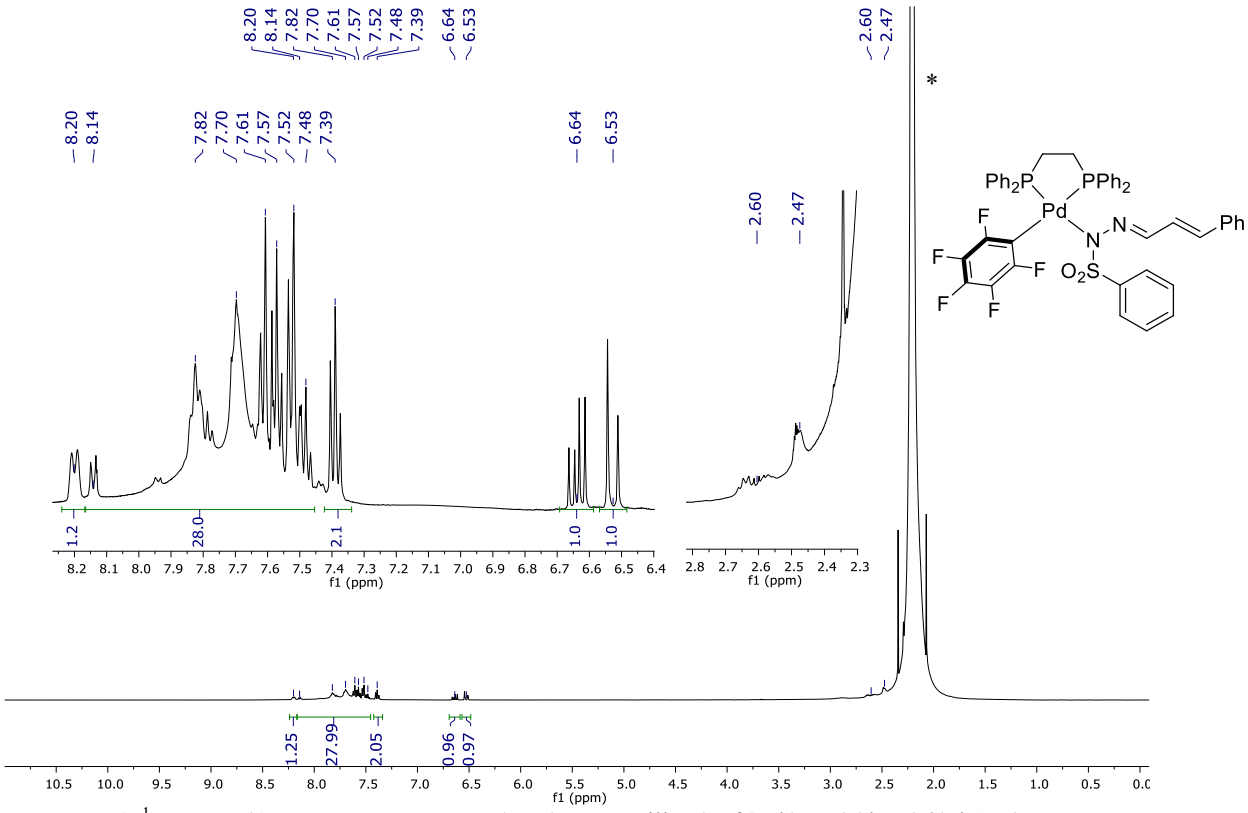

Figure S24. ^{1}H NMR (499.73 MHz, CH_3CN, $(CD_3)_2SO$ capillary) of [Pd(C_6F_5)(dppe){($PhSO_2$)N-N=CH-CH=CHPh}] (**5a-SO_2Ph**) generated in situ at 298 K. * Signal corresponding to the solvent (CH_3CN).

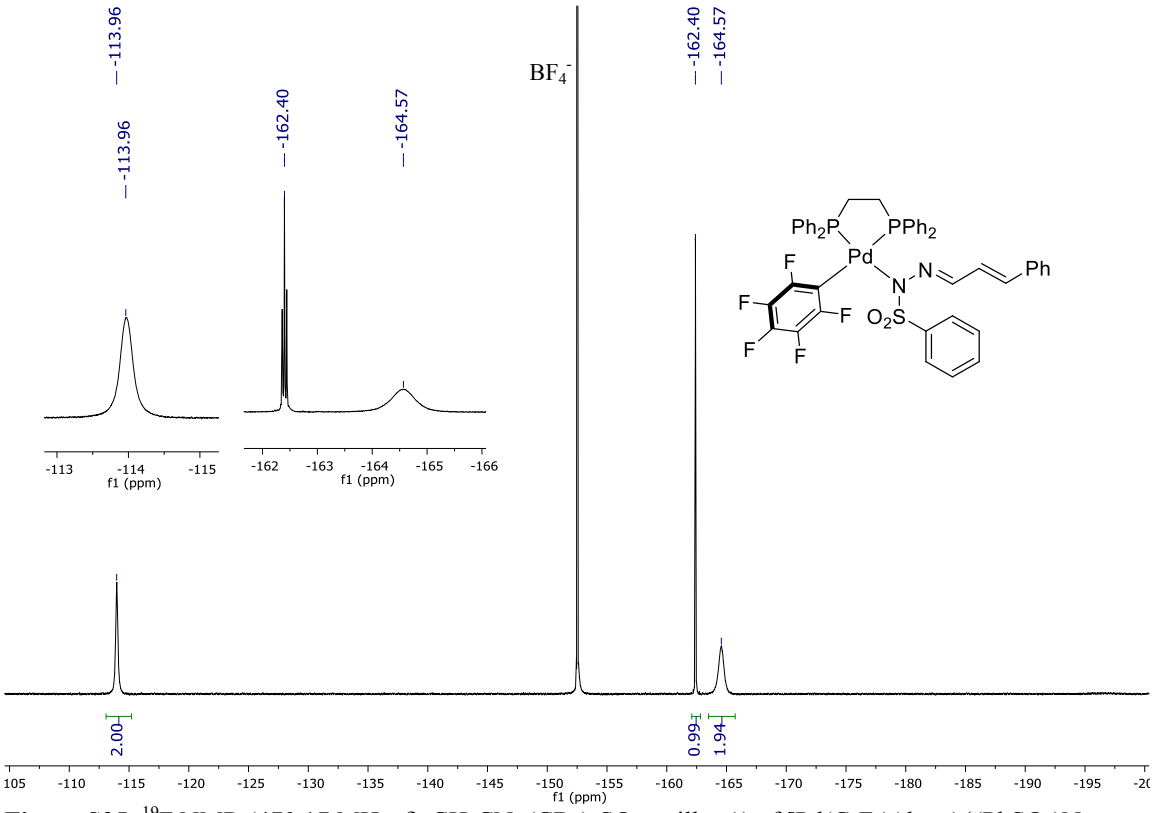

Figure S25. ^{19}F NMR (470.17 MHz, δ, CH_3CN, $(CD_3)_2SO$ capillary)) of [Pd(C_6F_5)(dppe){($PhSO_2$)N-N=CH-CH=CHPh}] (**5a-SO$_2$Ph**) generated in situ at 298 K. The presence of BF_4^- comes from the in situ generation of the $CsBF_4$ salt.

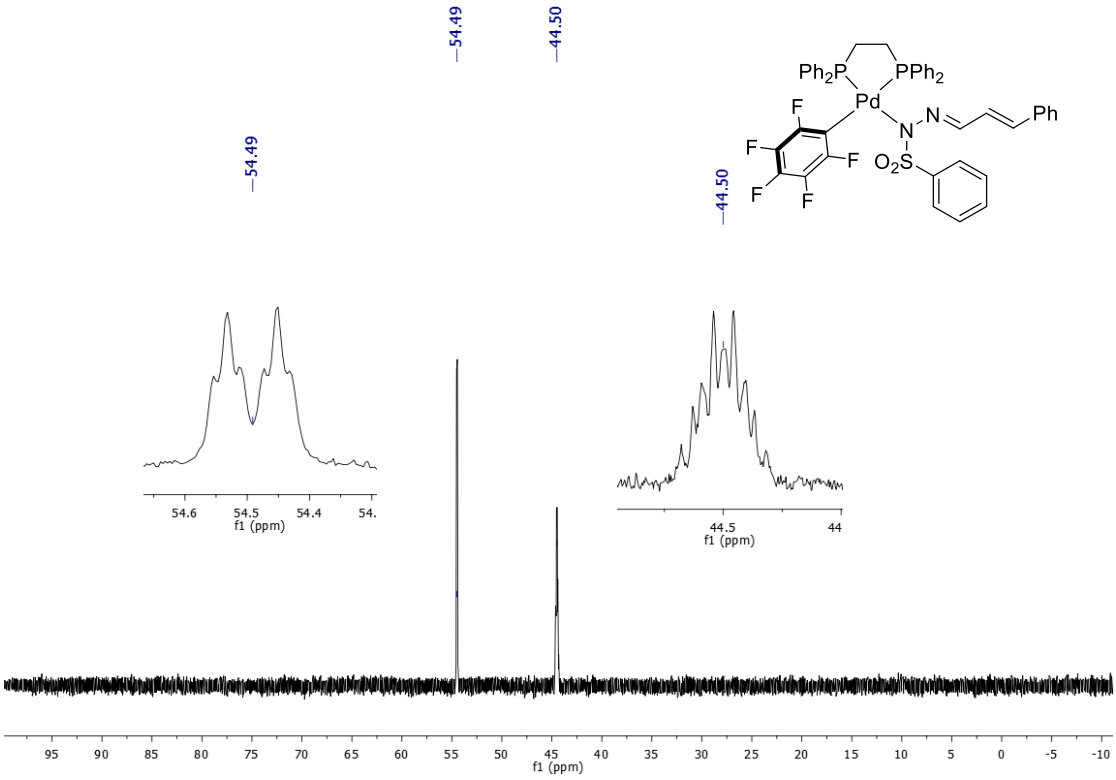

Figure S26. ^{31}P{^{1}H} NMR (202.31, MHz, δ, CH_3CN,$(CD_3)_2SO$ capillary) of [Pd(C_6F_5)(dppe){($PhSO_2$)N-N=CH-CH=CHPh}] (**5a-SO$_2$Ph**) generated in situ at 298 K.

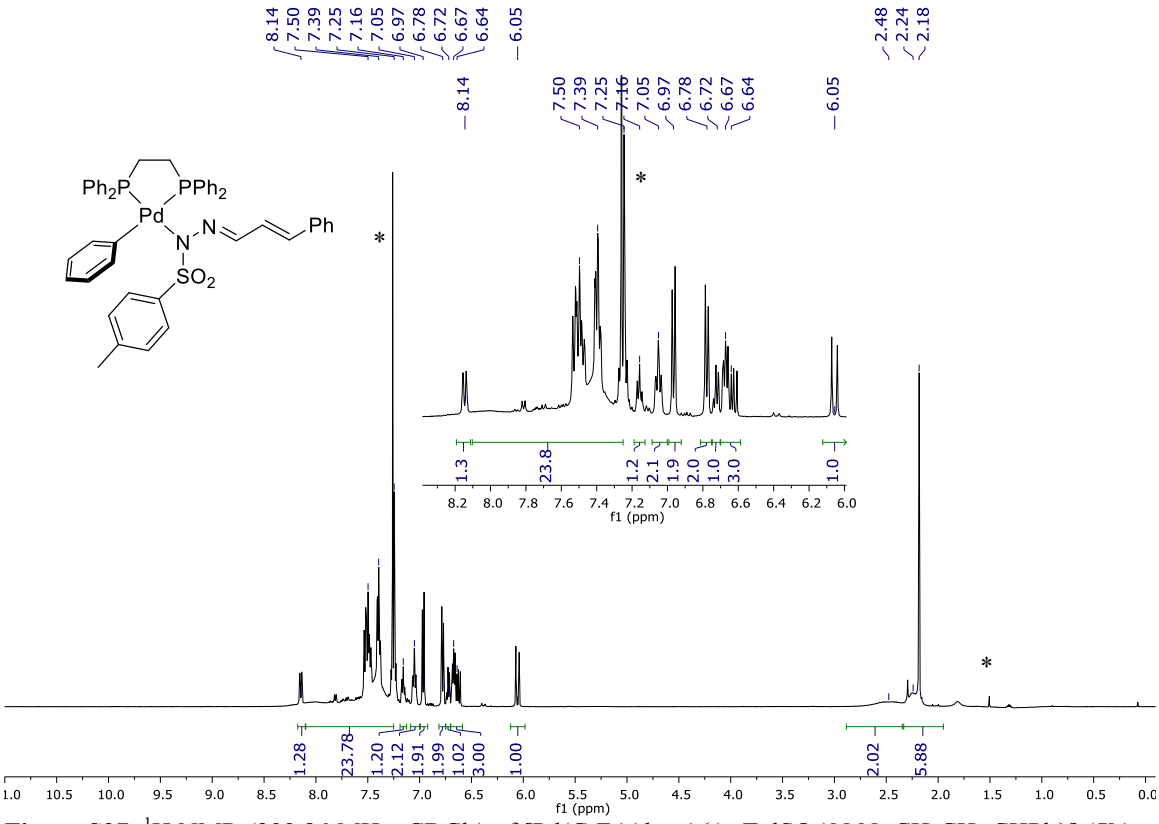

Figure S27. ^{1}H NMR (399.86 MHz, $CDCl_3$) of [Pd(C_6F_5)(dppe){(*p*-TolSO_2)N-N=CH-CH=CHPh}] (**5b**). * Signals corresponding to the solvent (H_2O and chloroform).

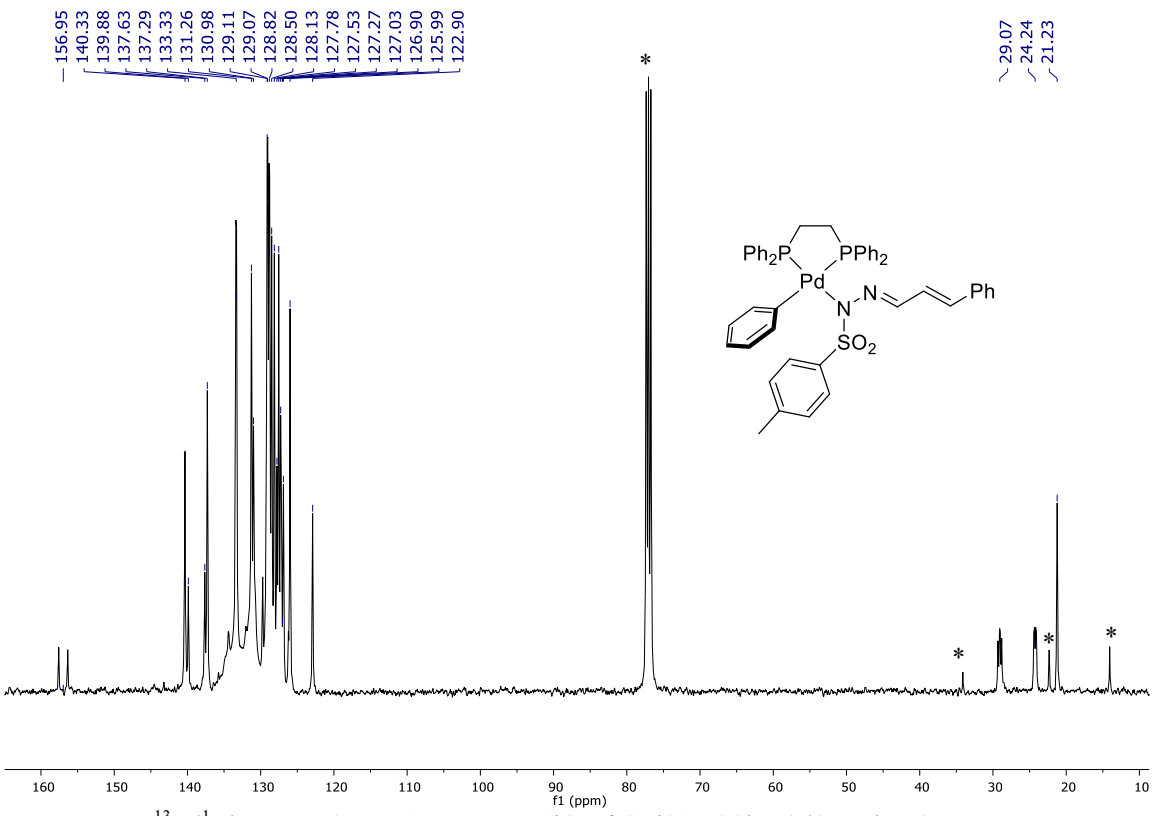

Figure S28. ^{13}C{^{1}H} NMR (100.56 MHz, $CDCl_3$) of [Pd(C_6F_5)(dppe){(*p*-TolSO_2)N-N=CH-CH=CH-Ph}] (**5b**). * Signals corresponding to the solvent (chloroform and hexane).

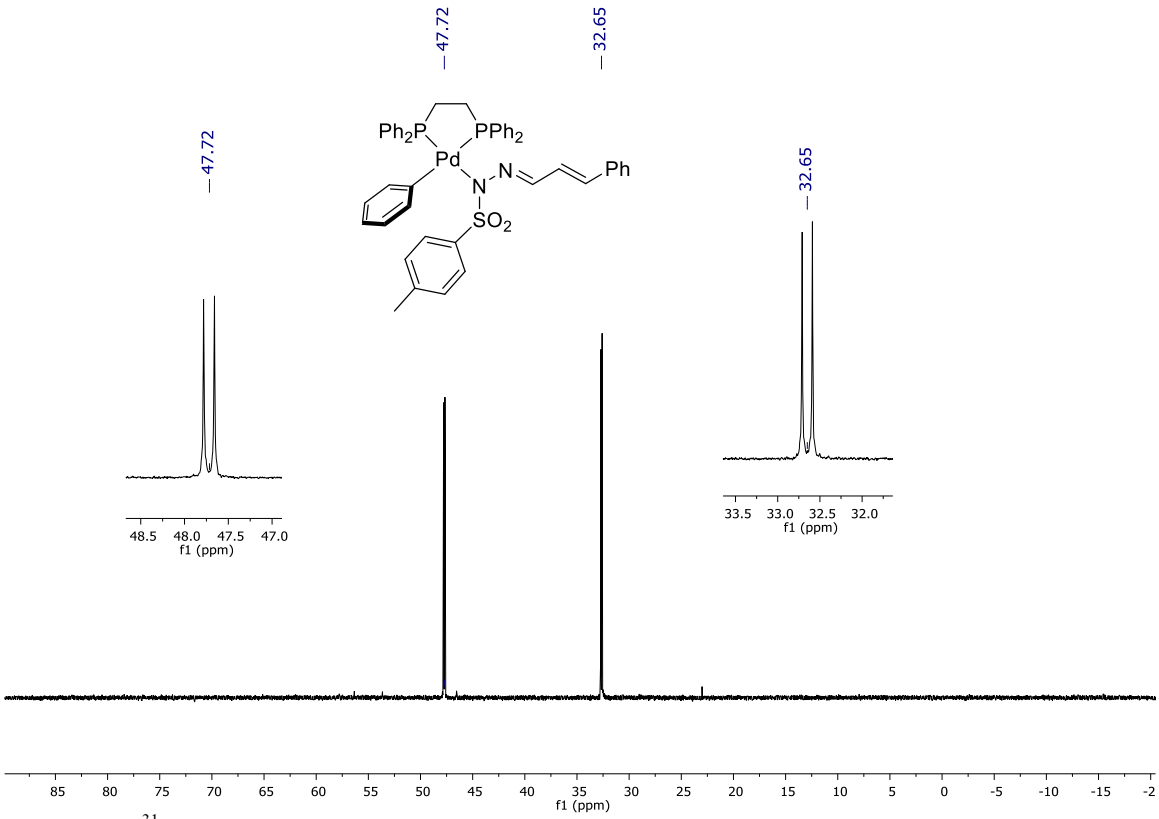

Figure S29. ^{31}P NMR (161.87 MHz, $CDCl_3$) of [Pd(C_6F_5)(dppe){(*p*-TolSO_2)N-N=CH-CH=CHPh}] (**5b**) at 298 K.

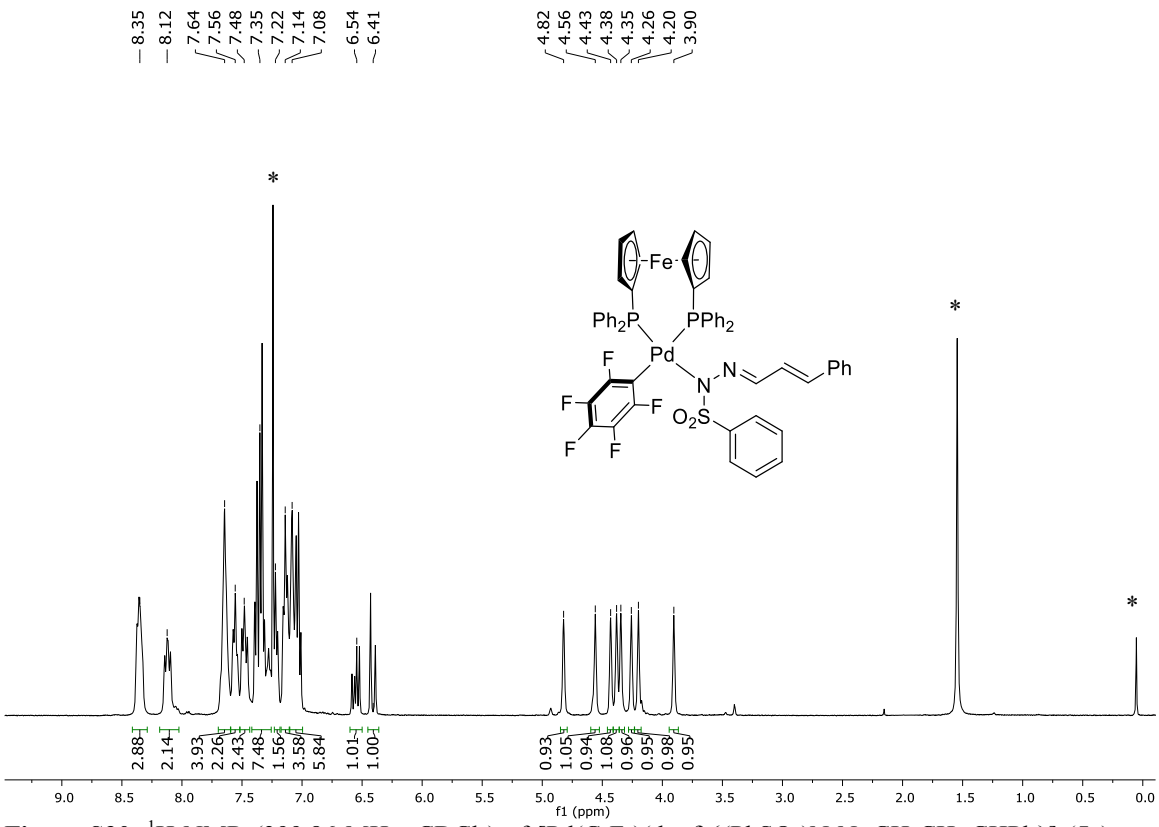

Figure S30. ^{1}H NMR (399.86 MHz, $CDCl_3$) of [Pd(C_6F_5)(dppf){($PhSO_2$)N-N=CH-CH=CHPh}] (**5c**) at 298 K. * Signals corresponding to the solvent (H_2O, chloroform and silicone grease).

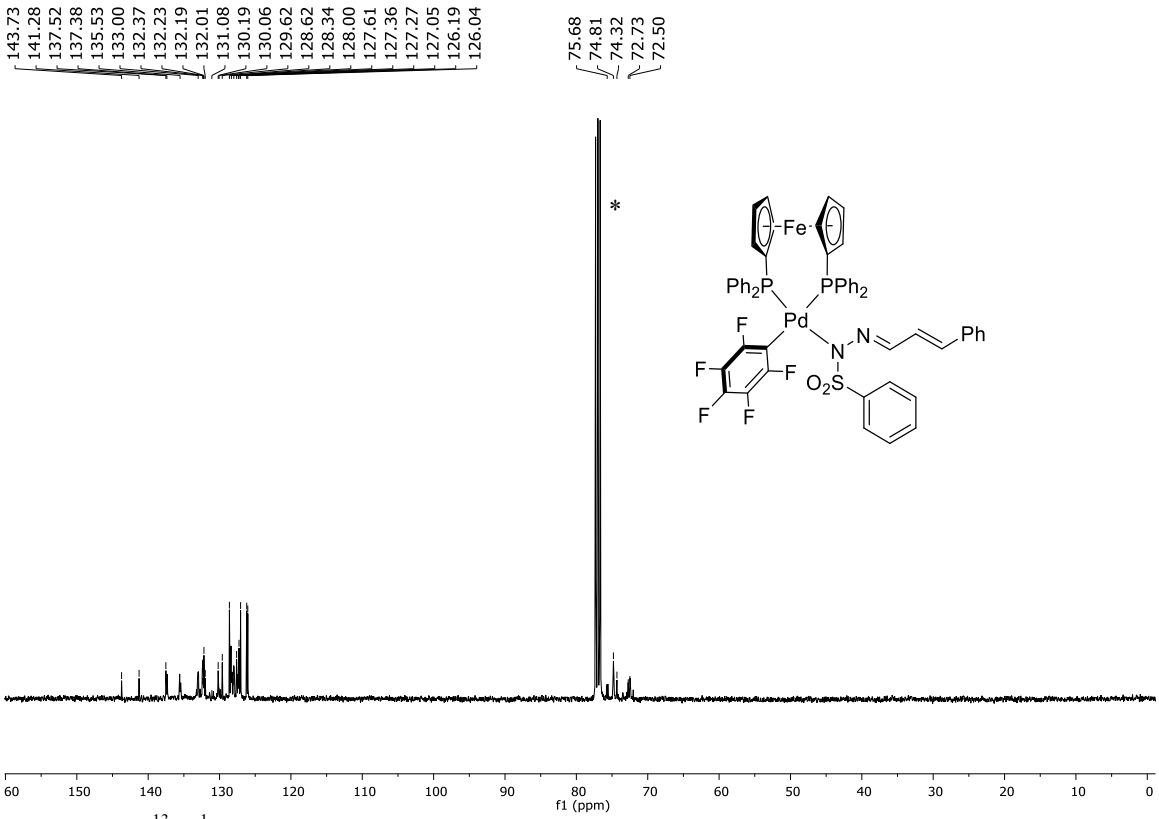

Figure S31. $^{13}C\{^{1}H\}$ NMR (100.56 MHz, $CDCl_3$) of $[Pd(C_6F_5)(dppf)\{(PhSO_2)N\text{-}N{=}CH\text{-}CH{=}CHPh\}]$ (**5c**) at 298 K. * Signals corresponding to the solvent (chloroform).

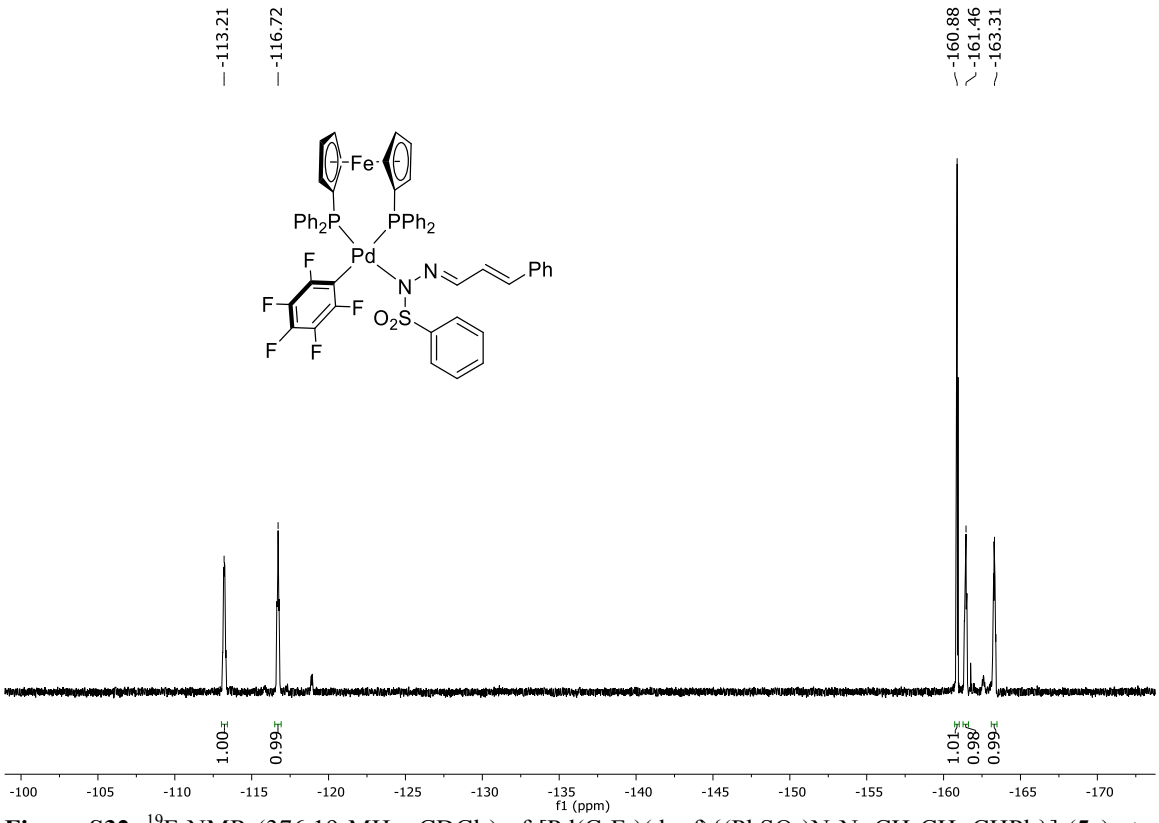

Figure S32. ^{19}F NMR (376.19 MHz, $CDCl_3$) of $[Pd(C_6F_5)(dppf)\{(PhSO_2)N\text{-}N{=}CH\text{-}CH{=}CHPh\}]$ (**5c**) at 298 K.

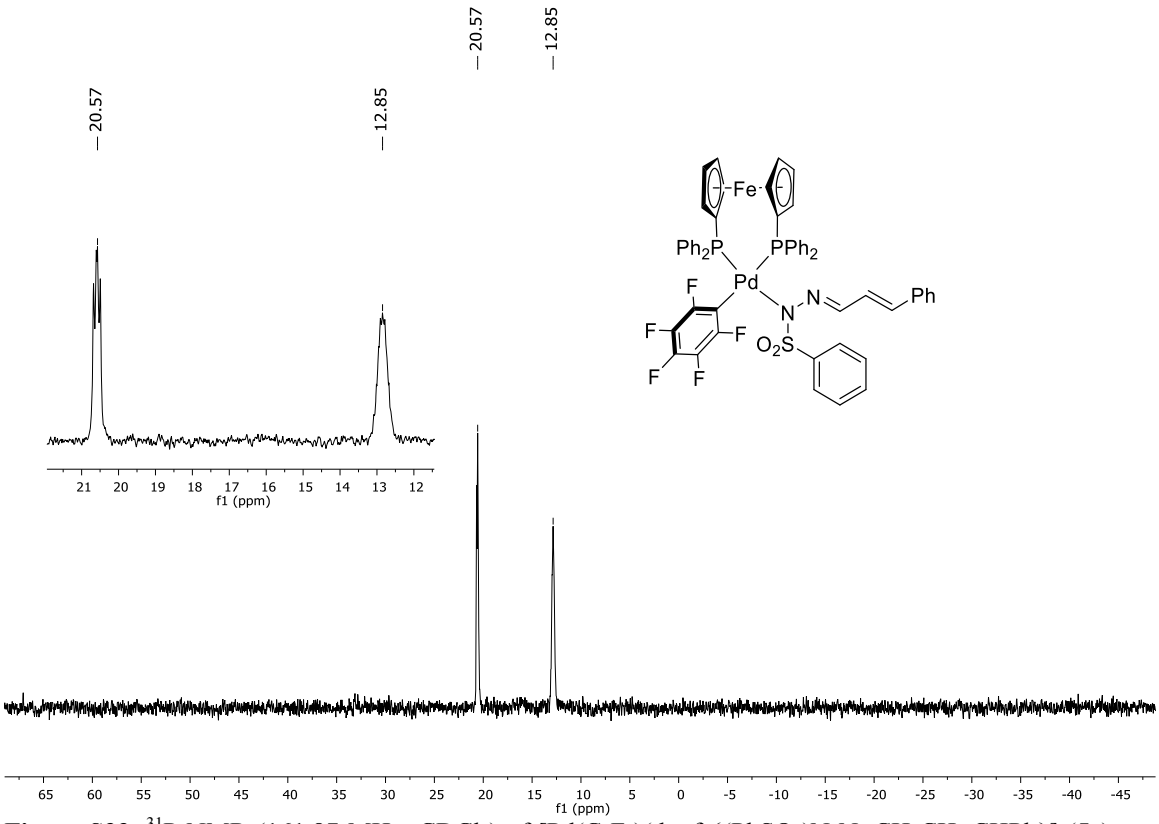

Figure S33. ^{31}P NMR (161.87 MHz, $CDCl_3$) of [Pd(C_6F_5)(dppf){($PhSO_2$)N-N=CH-CH=CHPh}] (**5c**) at 298 K.

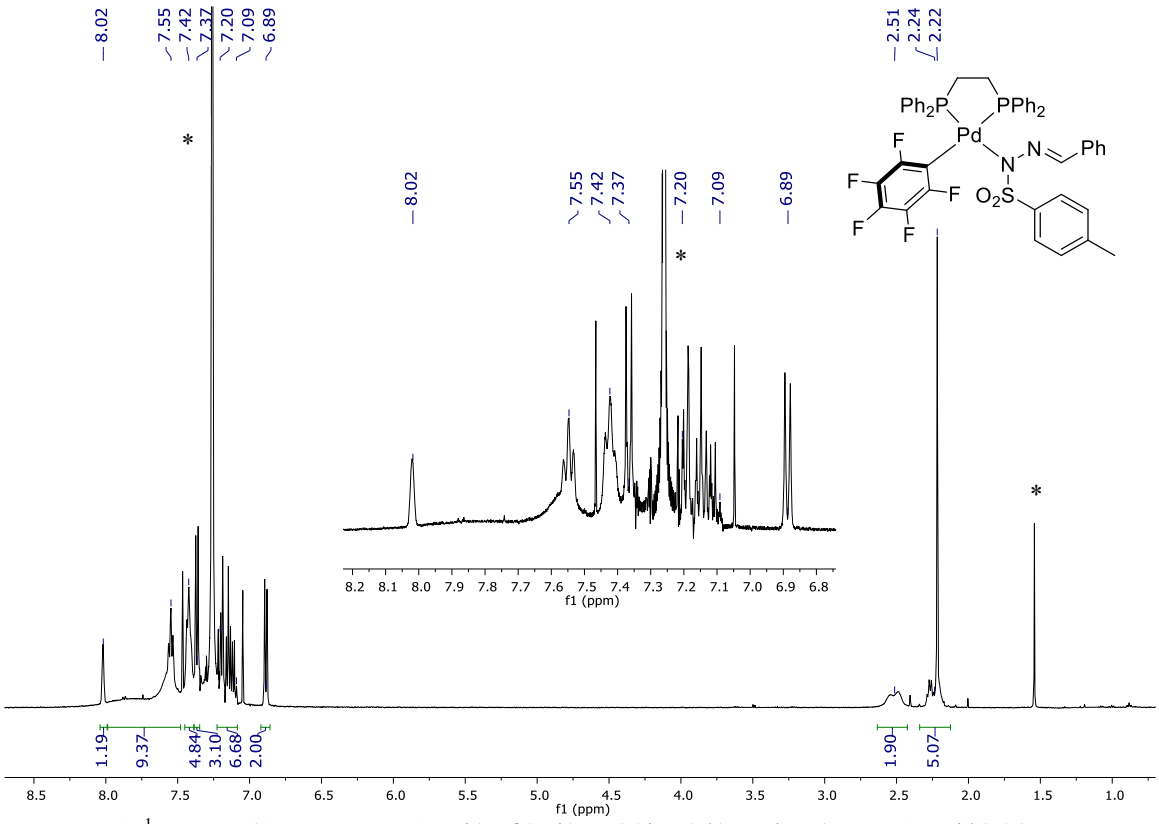

Figure S34. ^{1}H NMR (499.73 MHz, $CDCl_3$) of [Pd(C_6F_5)(dppe){(p-TolSO_2)N-N=CH-Ph}] (**6**) at 298 K. * Signals corresponding to the solvent (H_2O and chloroform).

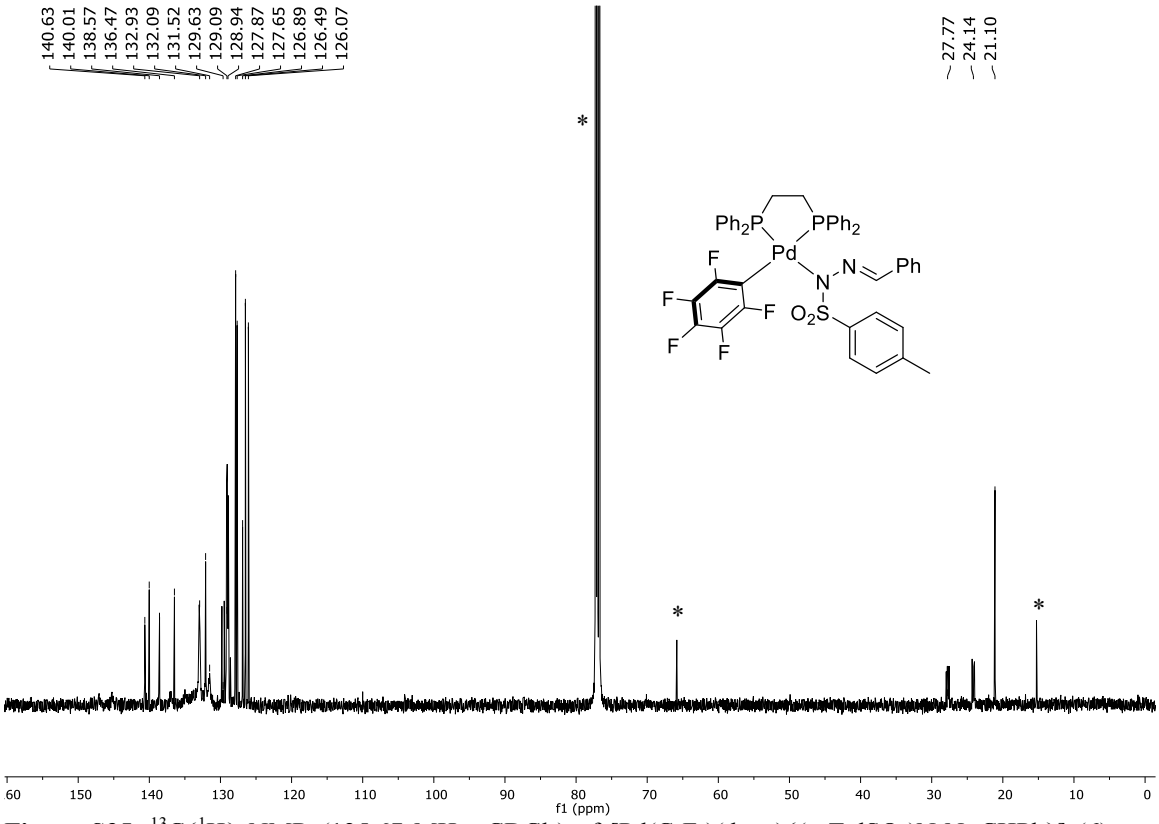

Figure S35. $^{13}C\{^{1}H\}$ NMR (125.67 MHz, $CDCl_3$) of [Pd(C_6F_5)(dppe){(*p*-TolSO_2)N-N=CHPh}] (**6**) at 298 K. * Signals corresponding to the solvent (diethyl-ether and chloroform).

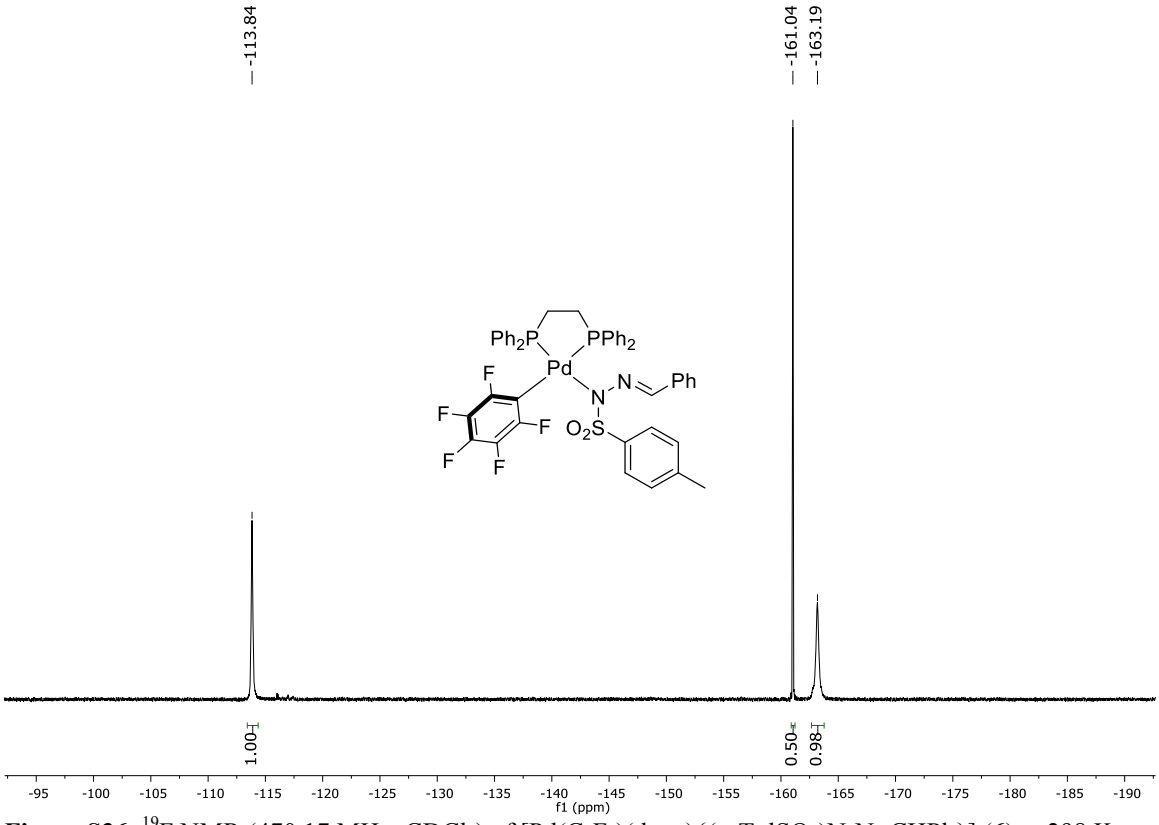

Figure S36. ^{19}F NMR (470.17 MHz, $CDCl_3$) of [Pd(C_6F_5)(dppe){(*p*-TolSO_2)N-N=CHPh}] (**6**) at 298 K.

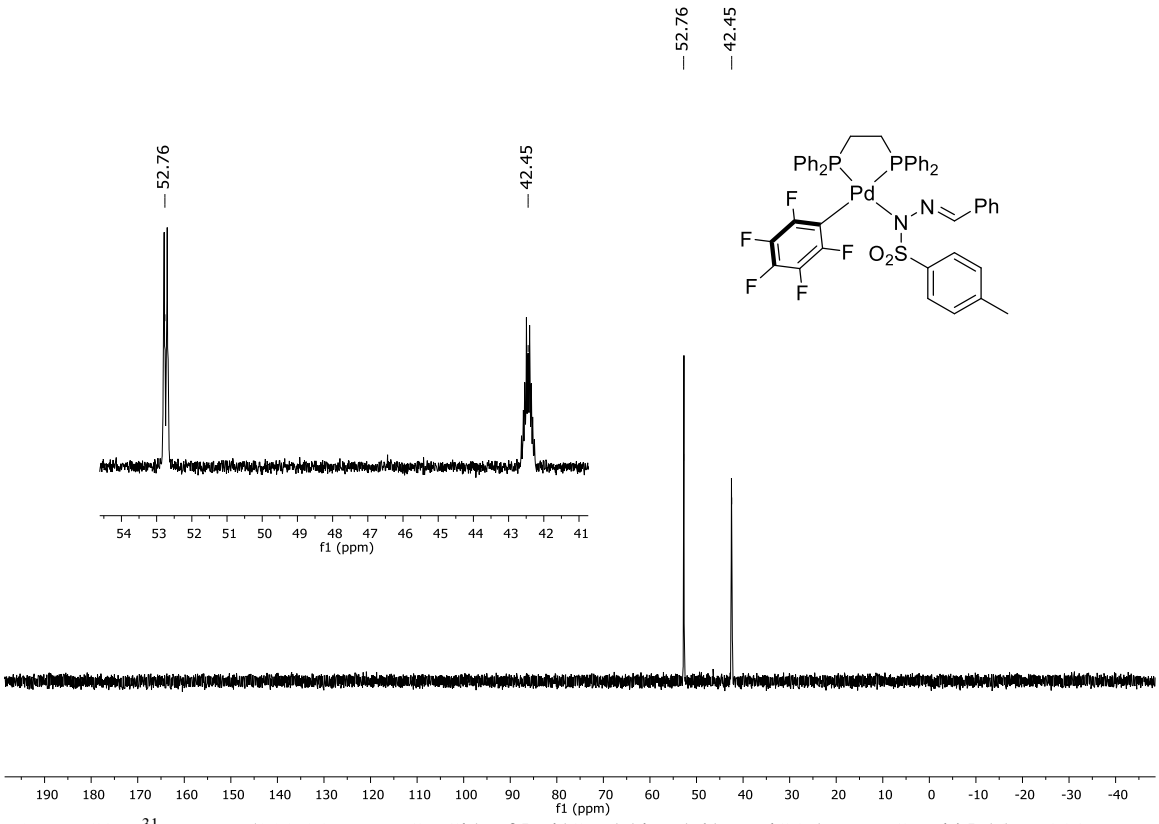

Figure S37. ^{31}P NMR (202.31 MHz, $CDCl_3$) of [Pd(C_6F_5)(dppe){(*p*-TolSO_2)N-N=CHPh}] (**6**) at 298 K.

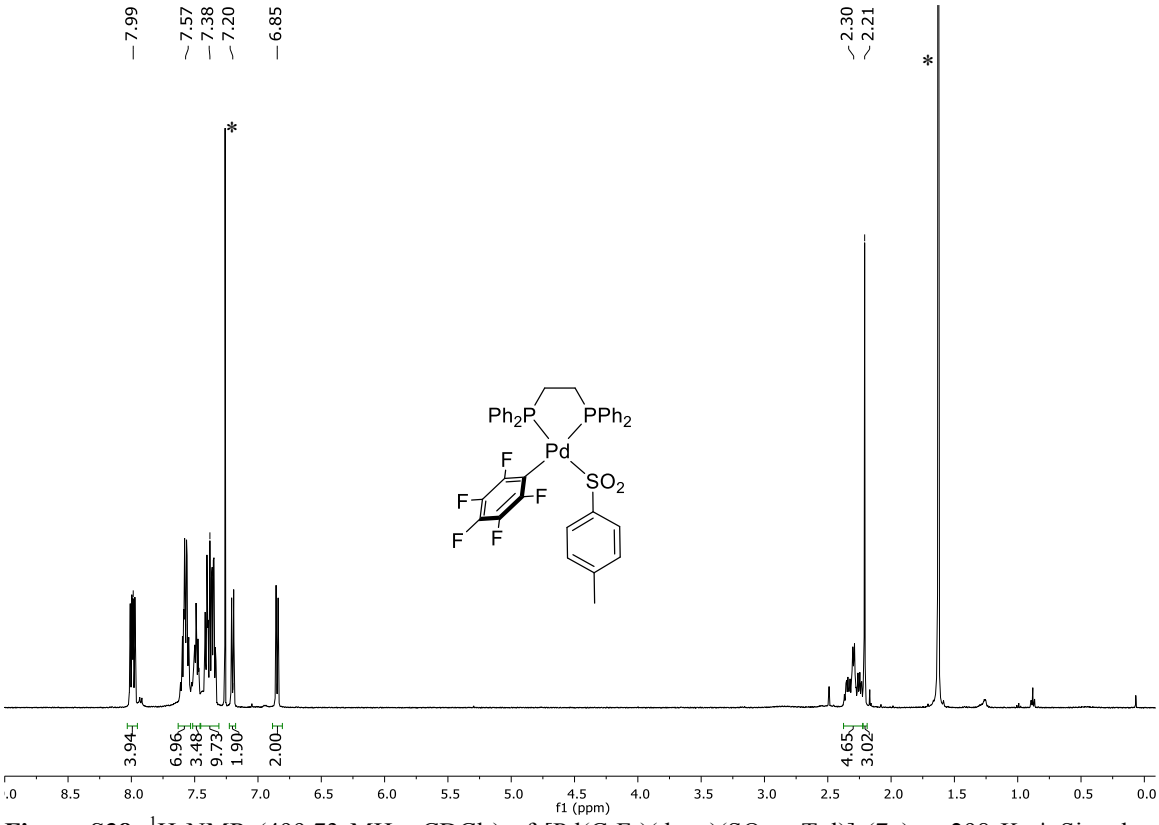

Figure S38. ^{1}H NMR (499.73 MHz, $CDCl_3$) of [Pd(C_6F_5)(dppe)(SO_2-p-Tol)] (**7a**) at 298 K. * Signals corresponding to the solvent (H_2O and chloroform).

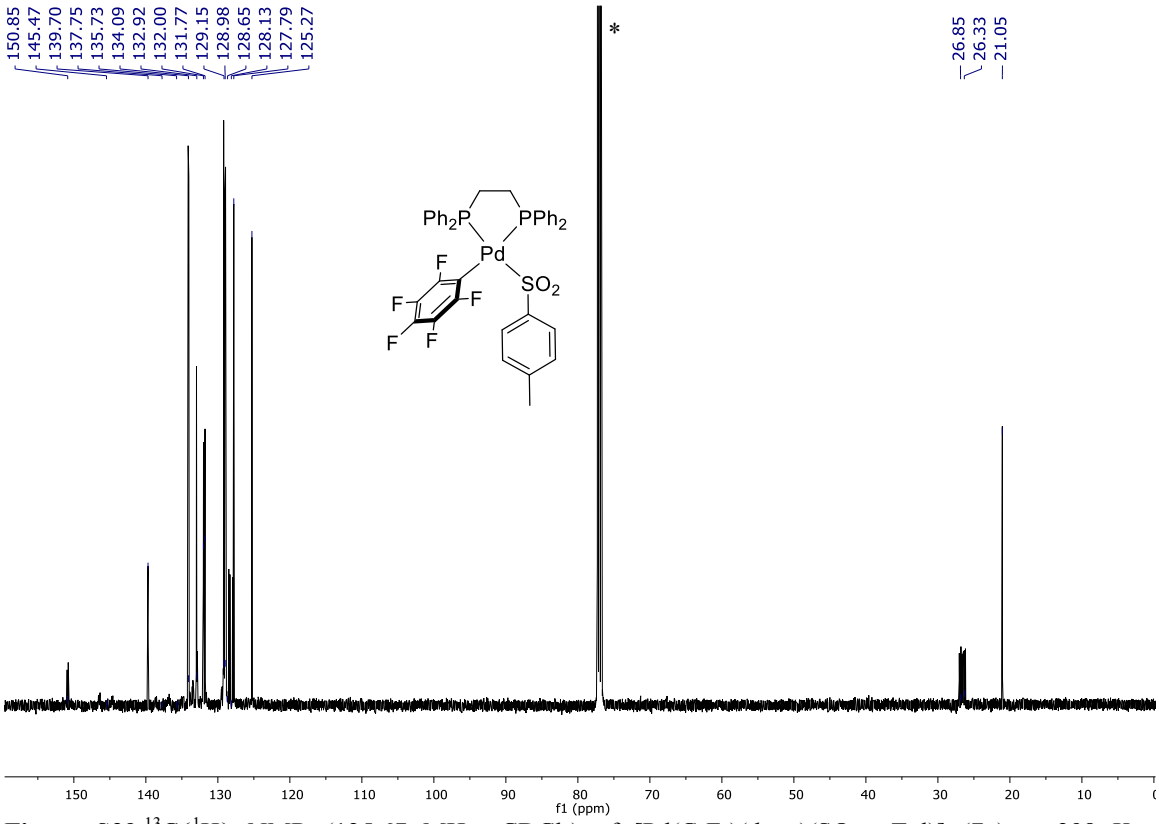

Figure S39. $^{13}C\{^{1}H\}$ NMR (125.67 MHz, $CDCl_3$) of $[Pd(C_6F_5)(dppe)(SO_2\text{-}p\text{-}Tol)]$ (**7a**) at 298 K. * Signals corresponding to the solvent (chloroform).

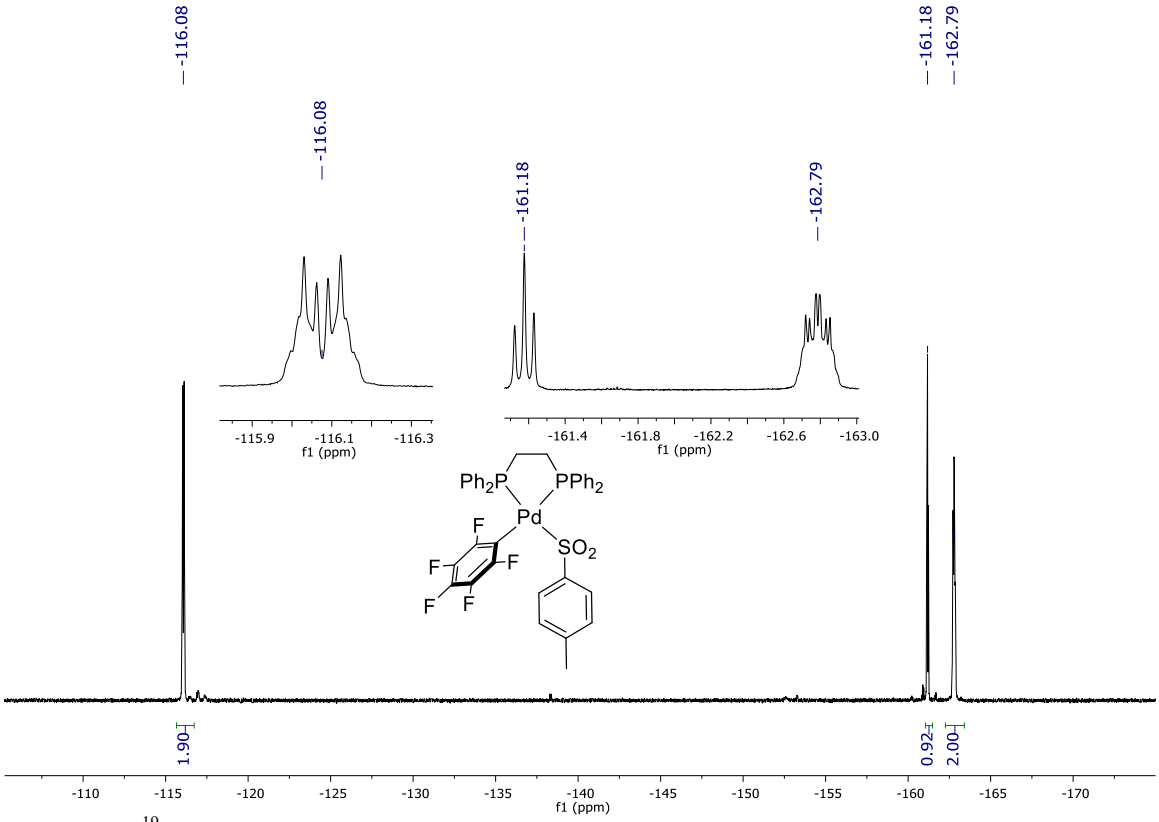

Figure S40. ^{19}F NMR (470.17 MHz, $CDCl_3$) of $[Pd(C_6F_5)(dppe)(SO_2\text{-}p\text{-}Tol)]$ (**7a**) at 298 K.

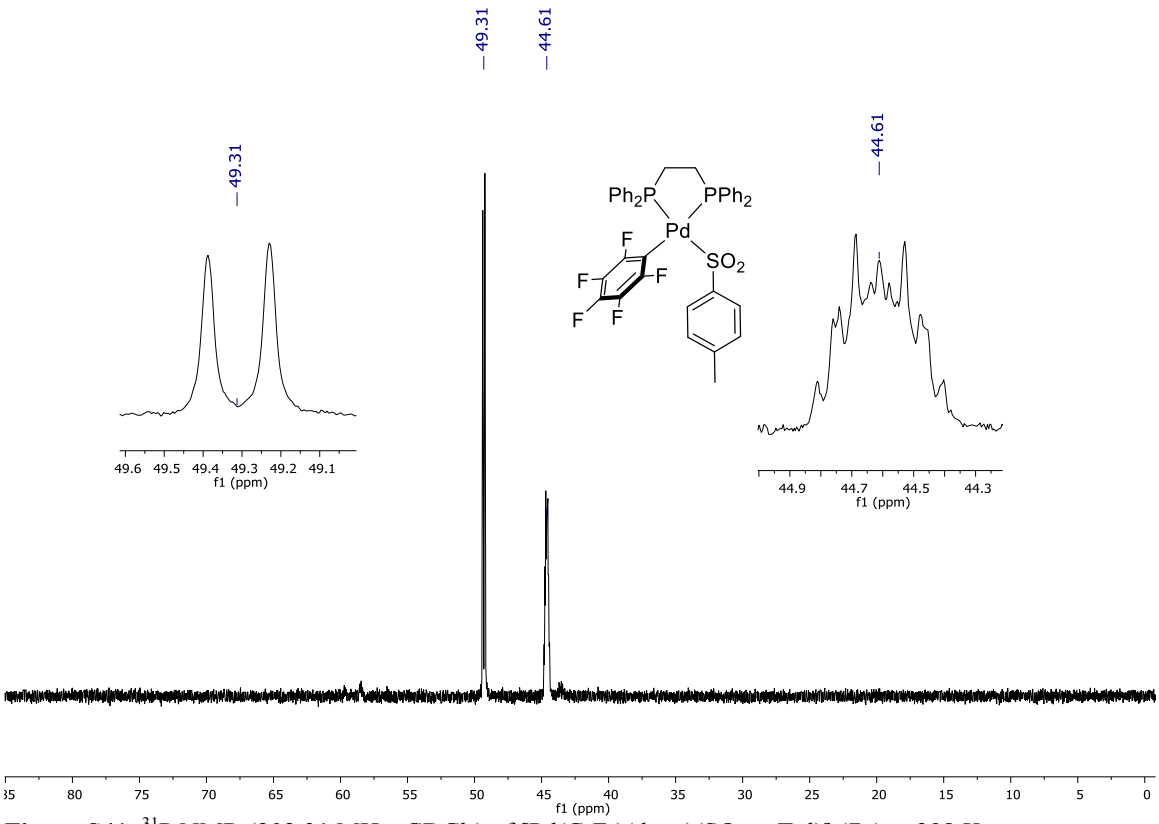

Figure S41. ^{31}P NMR (202.31 MHz, $CDCl_3$) of [Pd(C_6F_5)(dppe)(SO_2-p-Tol)] (**7a**) at 298 K.

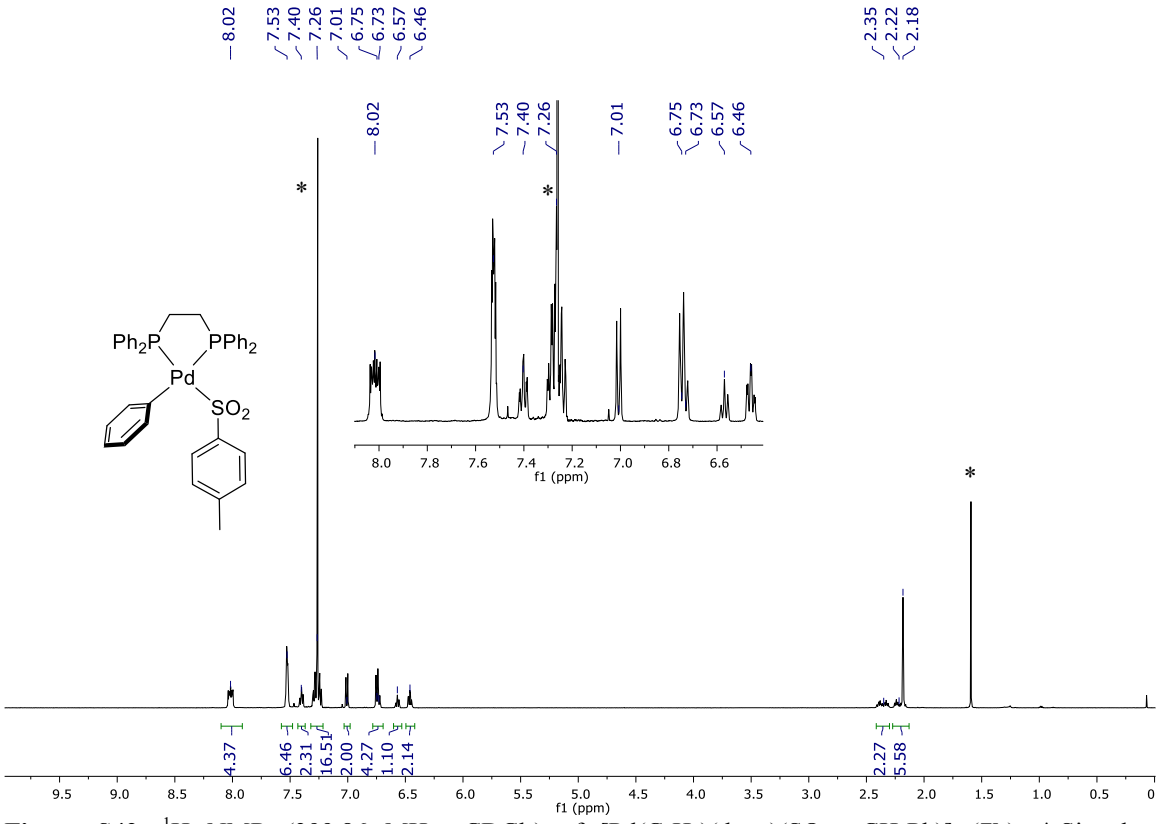

Figure S42. ^{1}H NMR (399.86 MHz, $CDCl_3$) of [Pd(C_6H_5)(dppe)(SO_2-*p*-CH_3Ph)] (**7b**). * Signals corresponding to the solvent (H_2O and chloroform).

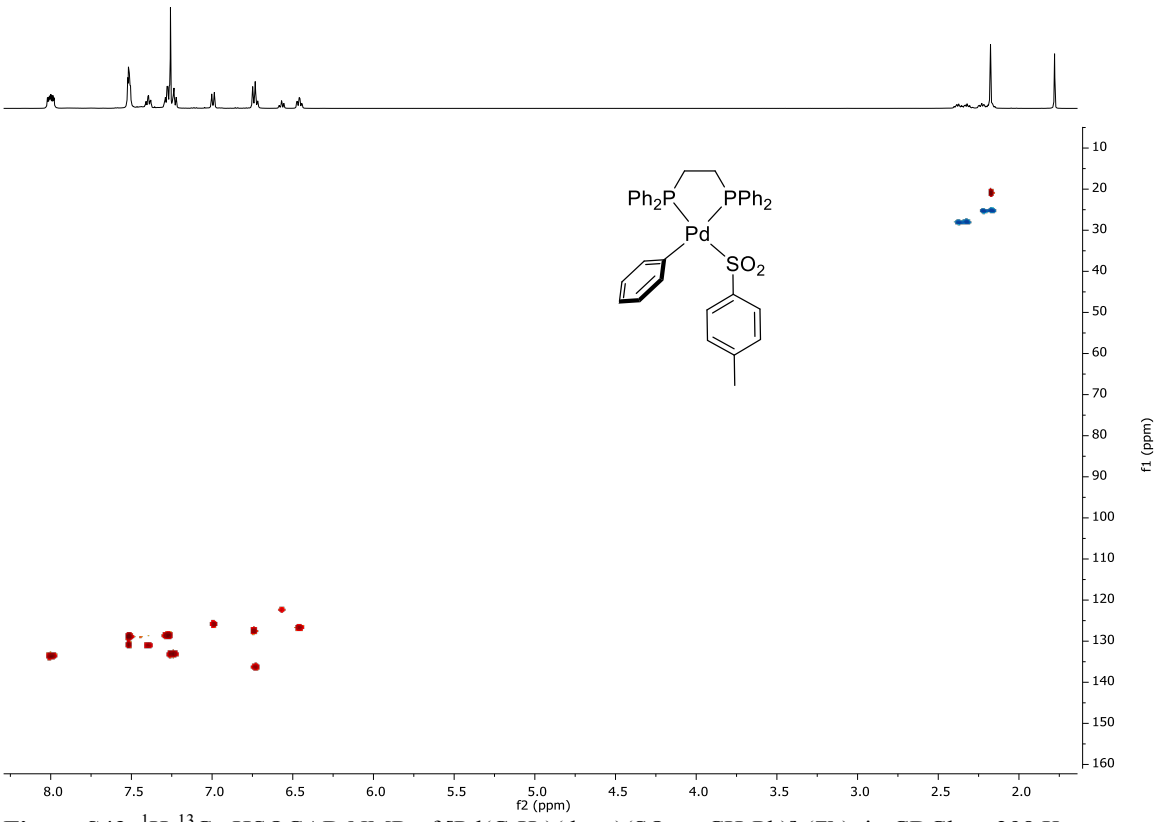

Figure S43. ^{1}H-^{13}C gHSQCAD NMR of [Pd(C_6H_5)(dppe)(SO_2-*p*-CH_3Ph)] (**7b**) in $CDCl_3$ at 298 K.

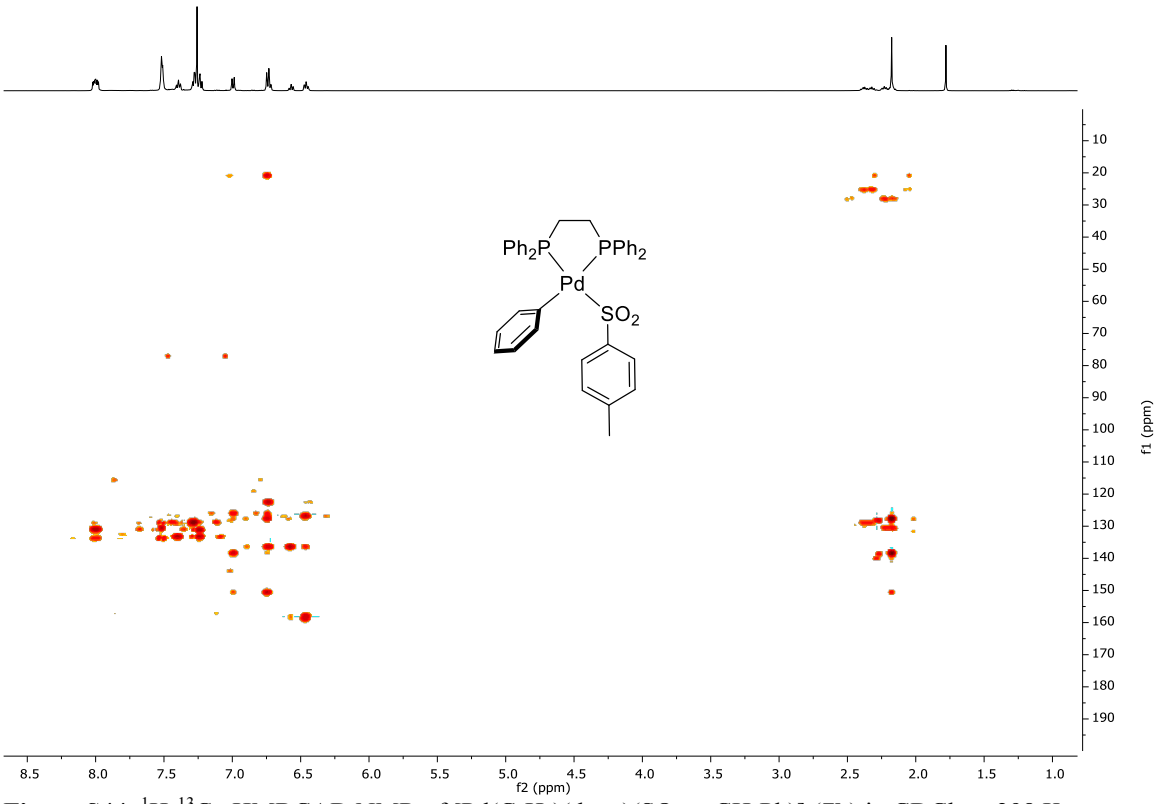

Figure S44. ^{1}H-^{13}C gHMBCAD NMR of [Pd(C_6H_5)(dppe)(SO_2-*p*-CH_3Ph)] (**7b**) in $CDCl_3$ at 298 K.

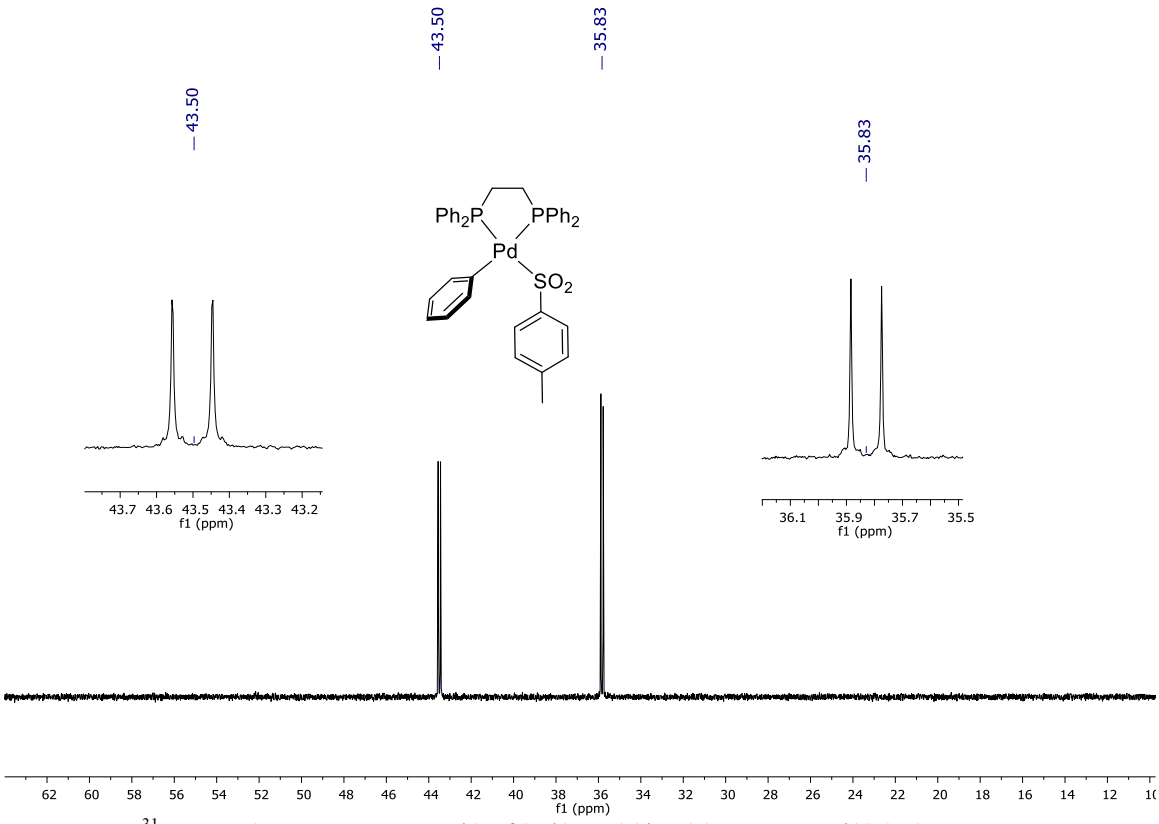

Figure S45. ^{31}P NMR (161.87 MHz, $CDCl_3$) of [Pd(C_6H_5)(dppe)(SO_2-*p*-CH_3Ph)] (**7b**) at 298 K.

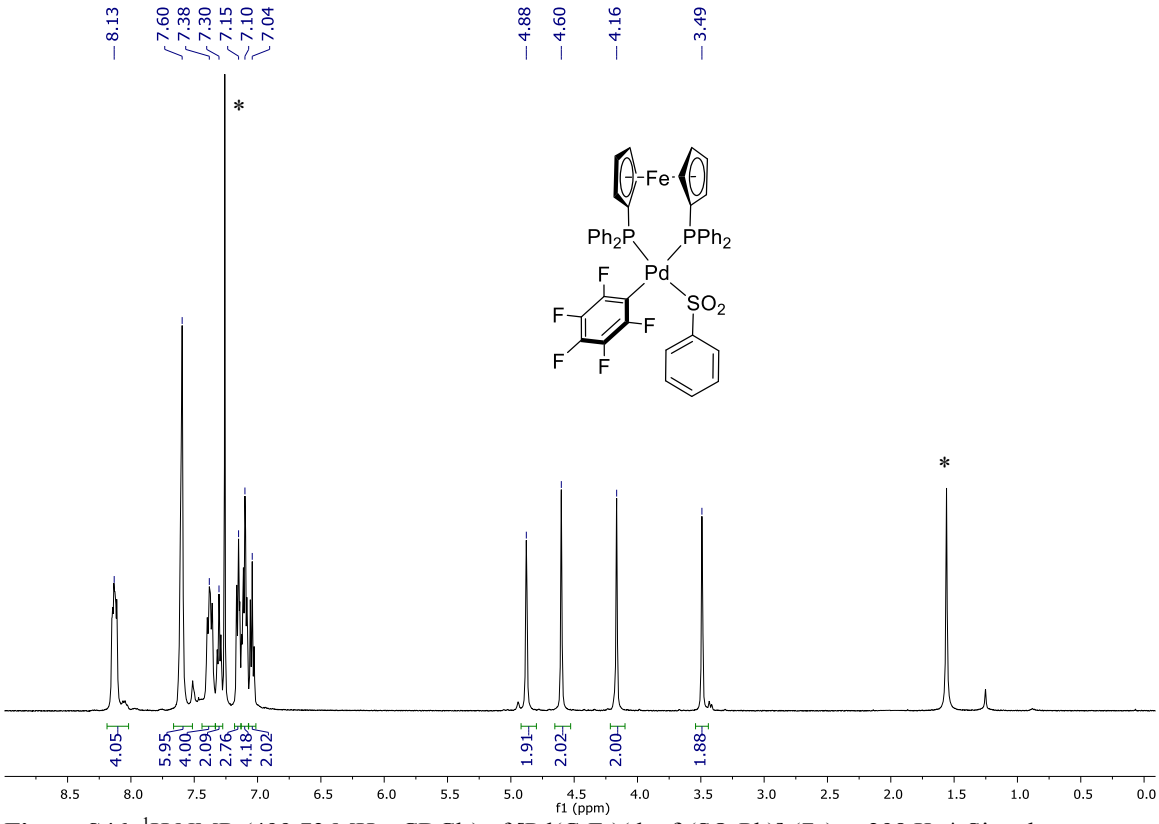

Figure S46. ^{1}H NMR (499.73 MHz, $CDCl_3$) of [Pd(C_6F_5)(dppf)(SO_2Ph)] (**7c**) at 298 K. * Signals corresponding to the solvent (H_2O and chloroform).

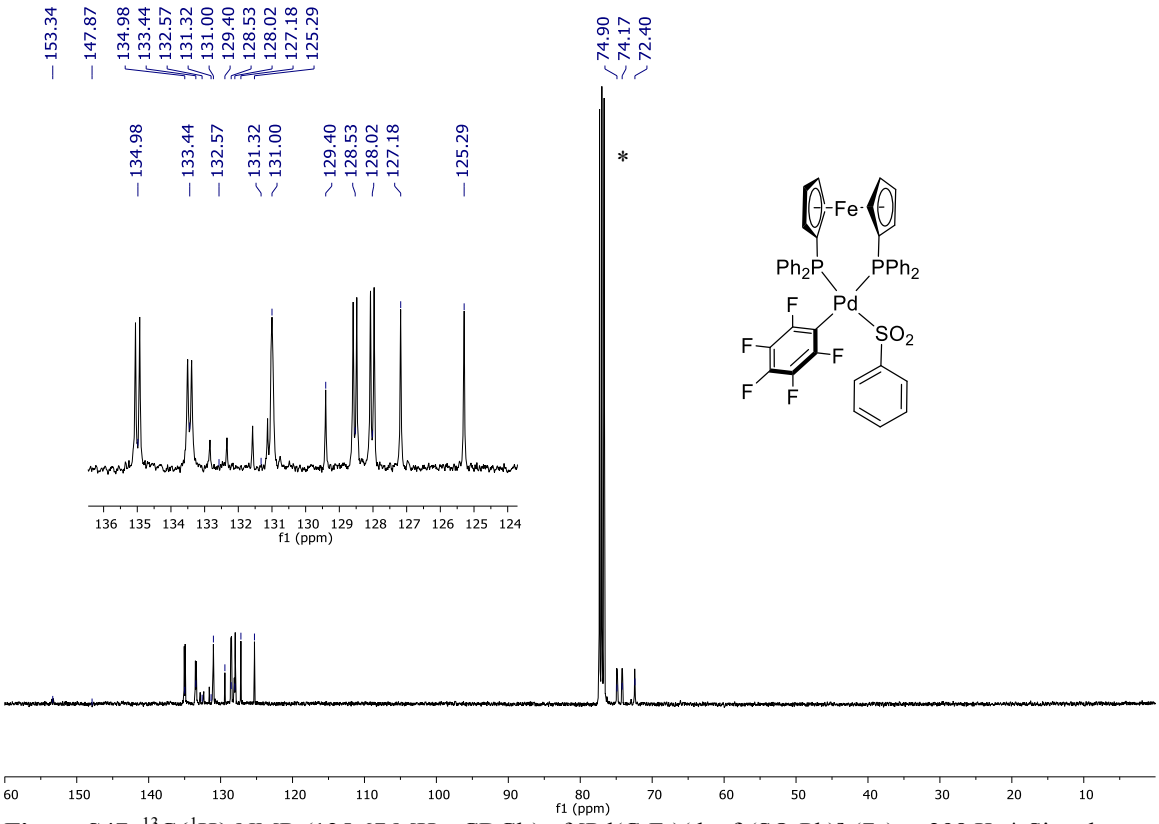

Figure S47. $^{13}C\{^{1}H\}$ NMR (125.67 MHz, $CDCl_3$) of **[**$Pd(C_6F_5)(dppf)(SO_2Ph)$] (**7c**) at 298 K. * Signals corresponding to the solvent (chloroform).

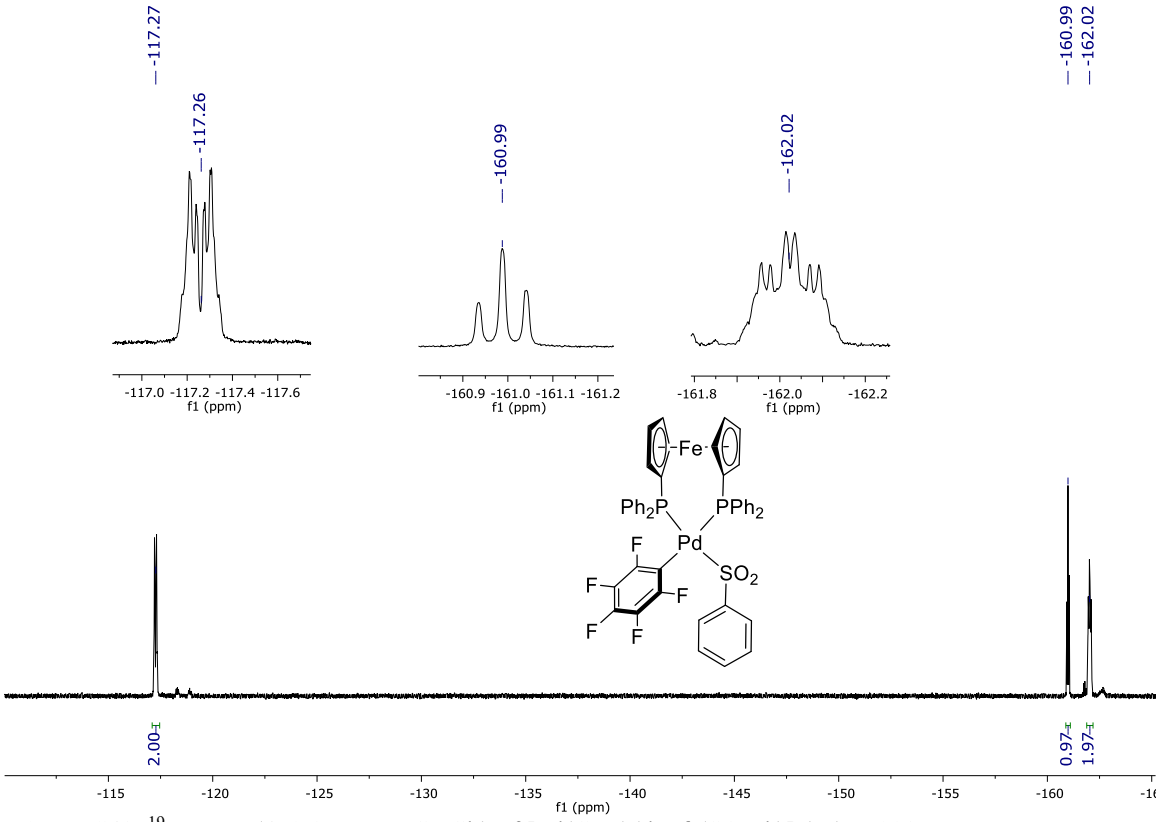

Figure S48. ^{19}F NMR (470.17 MHz, $CDCl_3$) of [$Pd(C_6F_5)(dppf)(SO_2Ph)$] (**7c**) at 298 K.

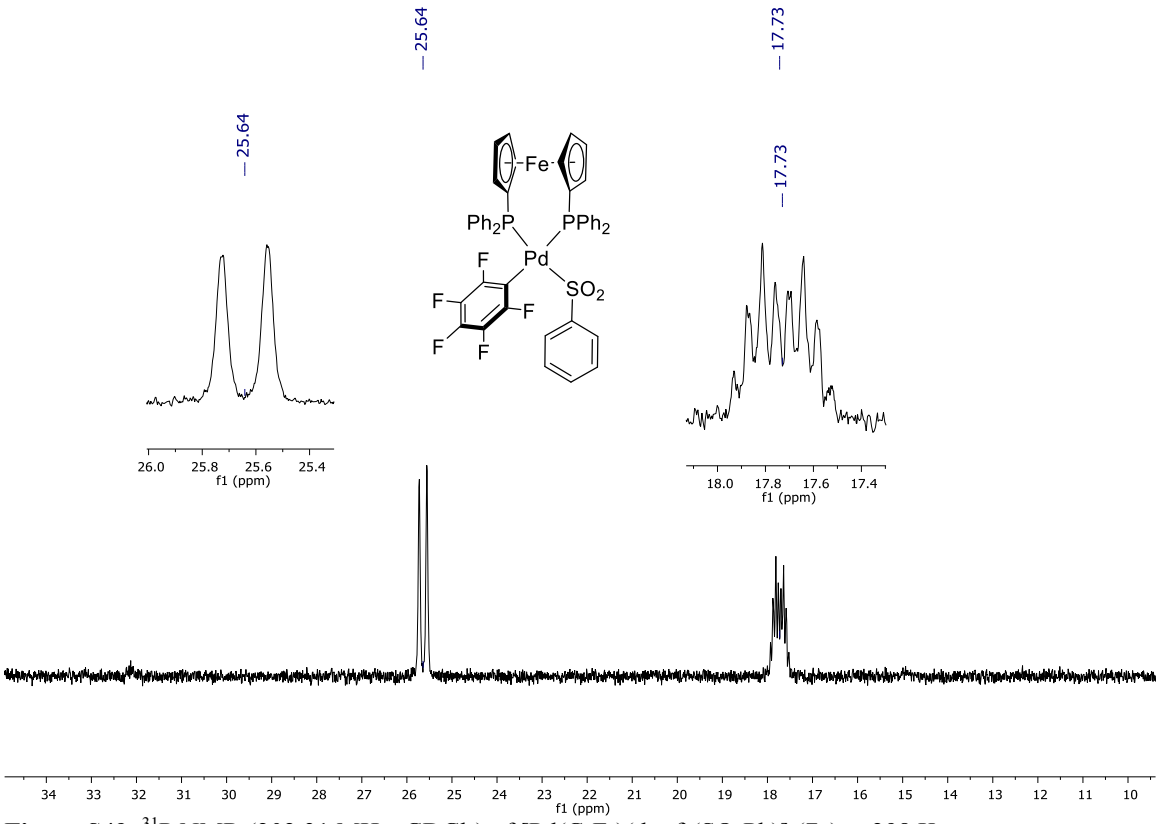

Figure S49. ^{31}P NMR (202.31 MHz, $CDCl_3$) of [Pd(C_6F_5)(dppf)(SO_2Ph)] (**7c**) at 298 K.

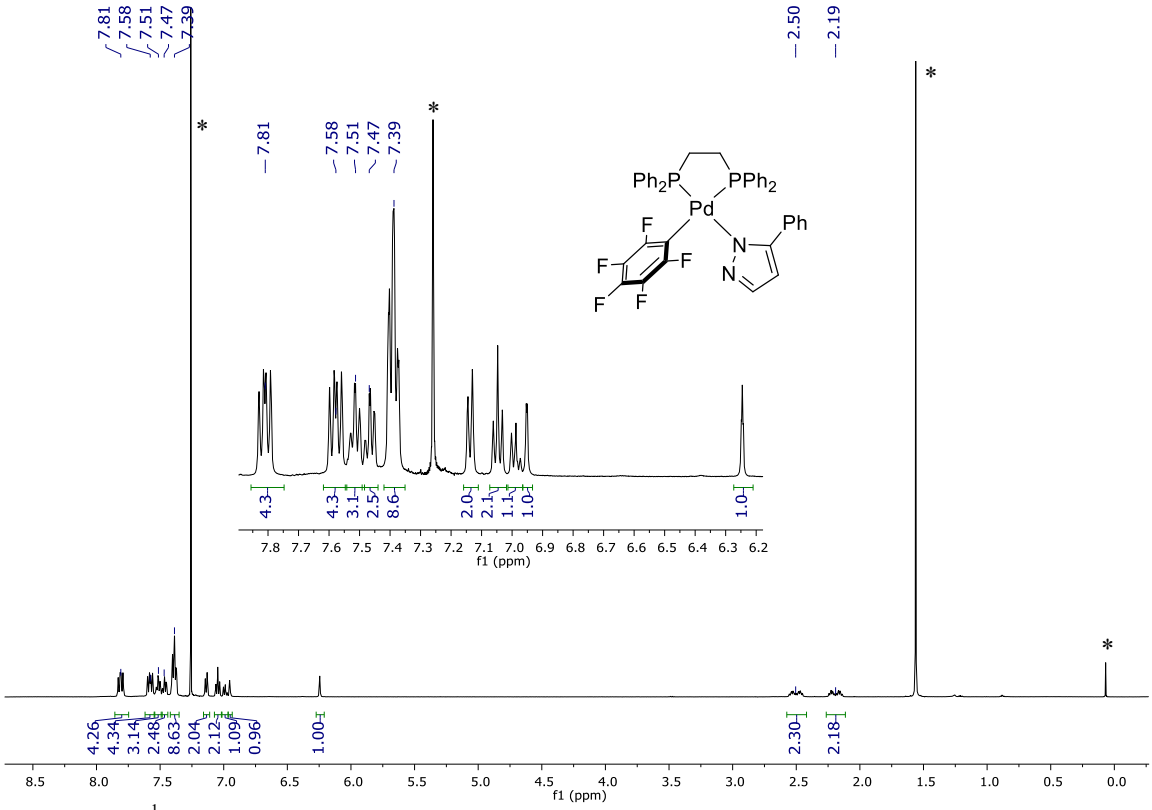

Figure S50. ^{1}H NMR (499.73 MHz, $CDCl_3$) of [Pd(C_6F_5)(dppe)($N_2C_3H_2$Ph)] (**8**) at 298 K. * Signals corresponding to the solvent (chloroform, H_2O and silicone grease).

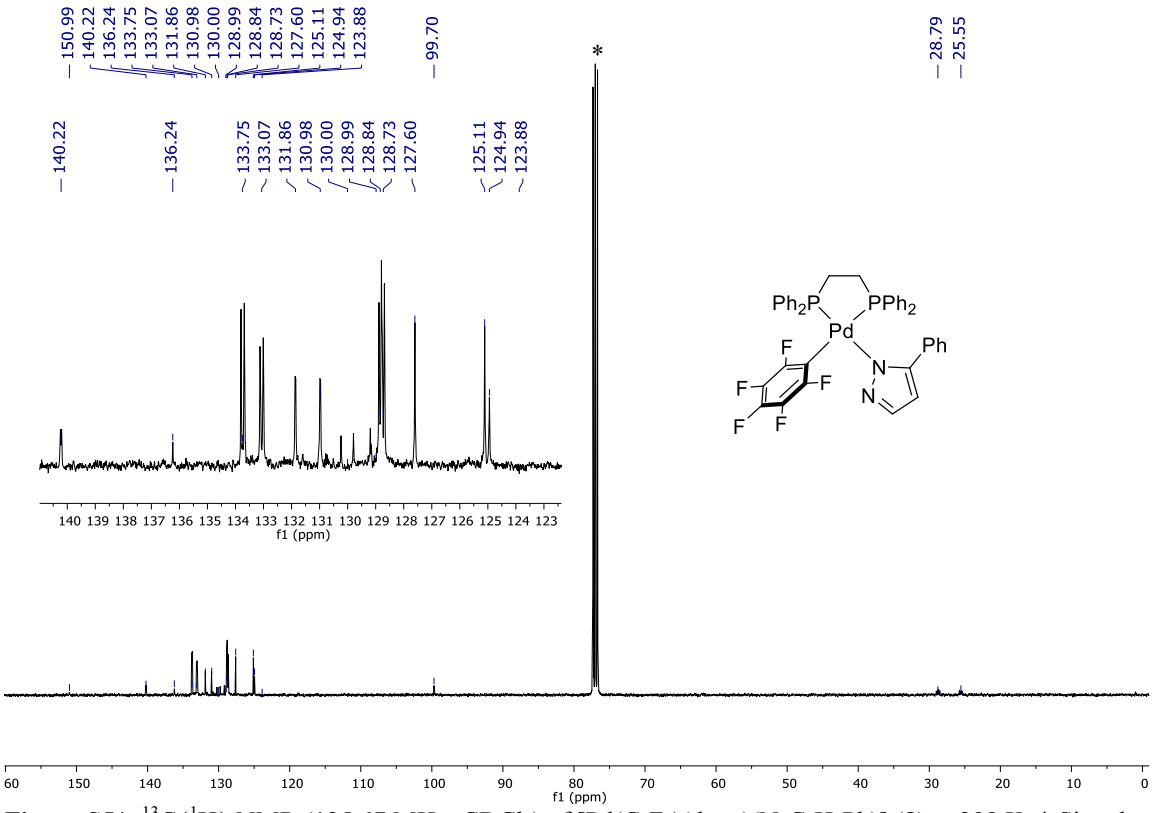

Figure S51. $^{13}C\{^{1}H\}$ NMR (125.67 MHz, $CDCl_3$) of $[Pd(C_6F_5)(dppe)(N_2C_3H_2Ph)]$ (**8**) at 298 K. * Signals corresponding to the solvent (chloroform).

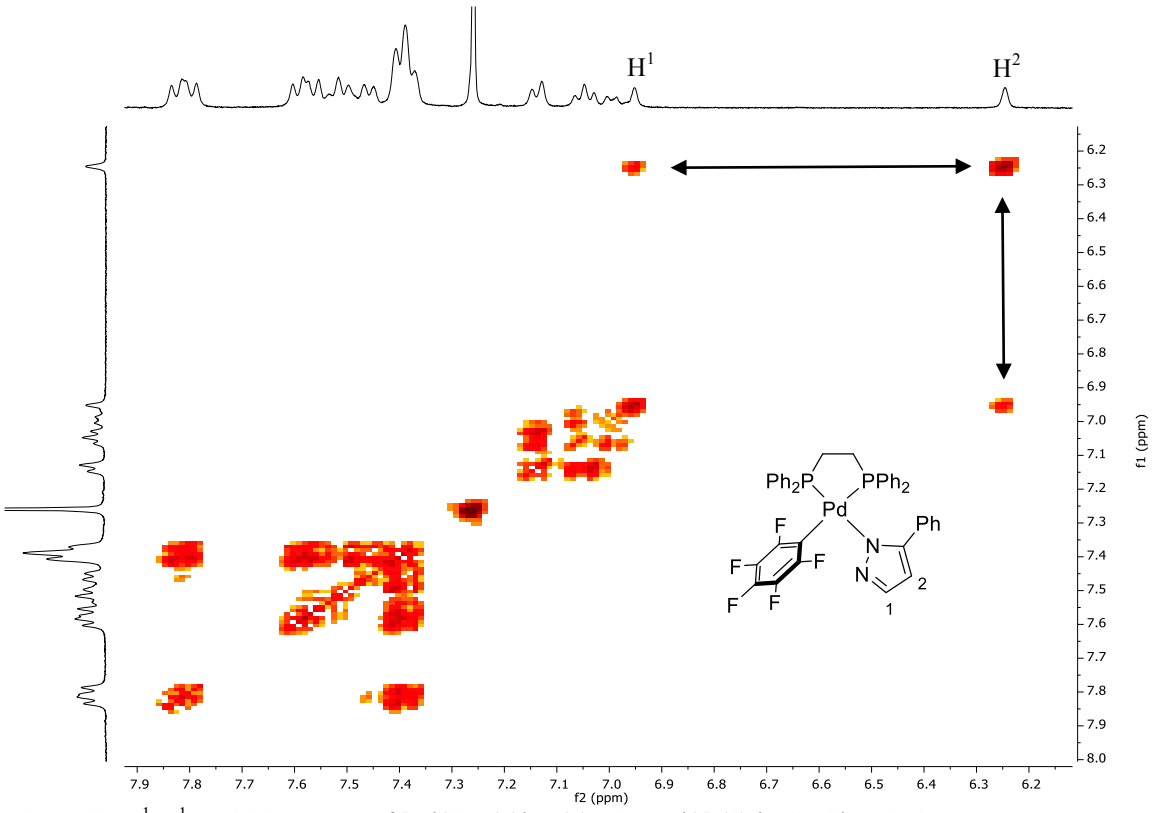

Figure S52. ^{1}H-^{1}H gCOSY NMR of $[Pd(C_6F_5)(dppe)(N_2C_3H_2Ph)]$ (**8**) in $CDCl_3$ at 298 K.

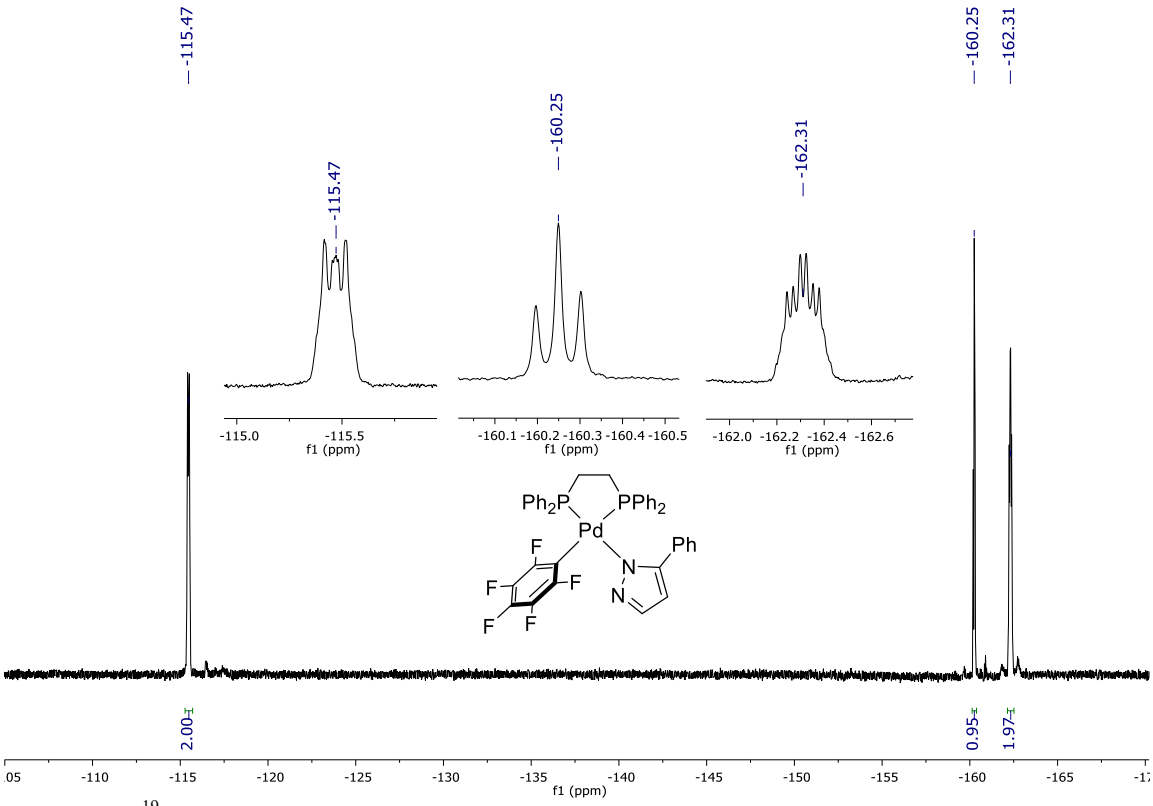

Figure S53. ^{19}F NMR (470.17 MHz, $CDCl_3$) of [Pd(C_6F_5)(dppe)($N_2C_3H_2Ph$)] (**8**) at 298 K**.**

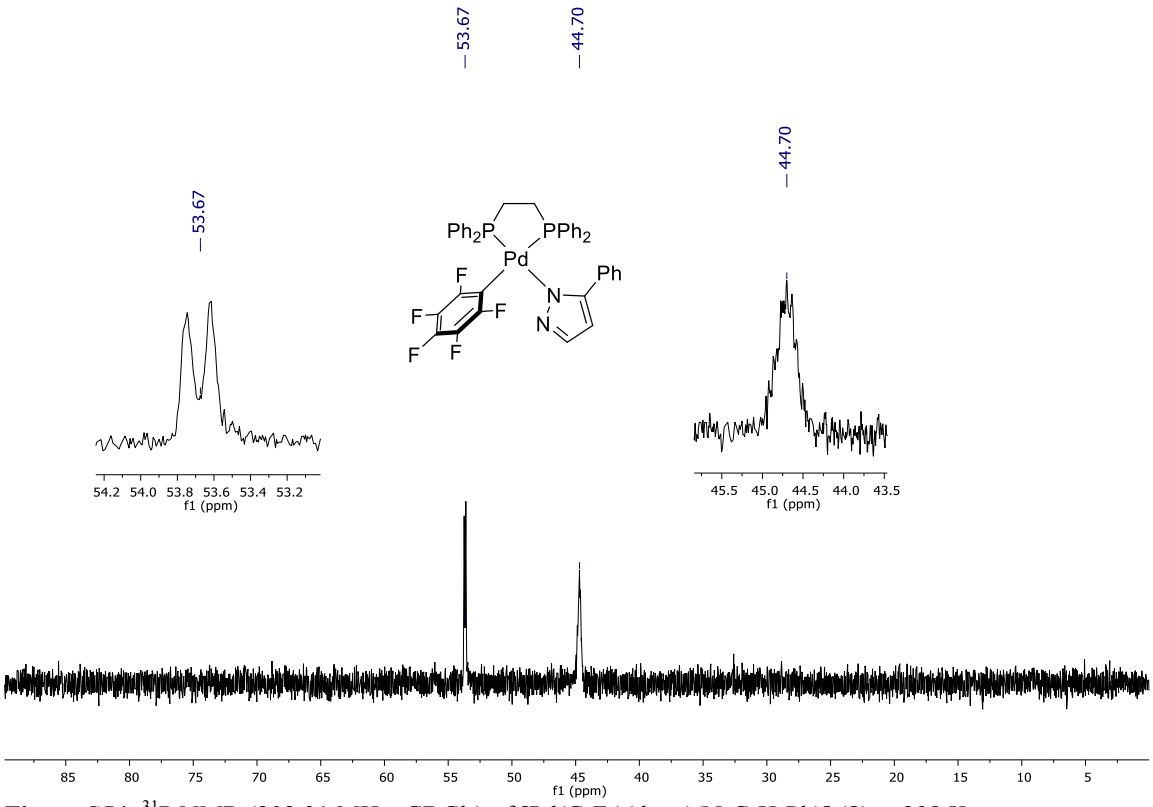

Figure S54. ^{31}P NMR (202.31 MHz, $CDCl_3$) of [Pd(C_6F_5)(dppe)($N_2C_3H_2Ph$)] (**8**) at 298 K.

4. References

1 J. Wen, Y. Fu, R.-Y. Zhang, J. Zhang, S.-Y. Chen, X.-Q. Yu, *Tetrahedron* 2011, **67**, 9618–9621.

2 N. V Russavskaya, V. A. Grabel'nykh, E. P. Levanova, E. N. Sukhomazova, E. N. Deryagina, *Russ. J. Org. Chem.* 2002, **38**, 1498–1500.